Research Square

Preprints are preliminary reports that have not undergone peer review.
They should not be considered conclusive, used to inform clinical practice,
or referenced by the media as validated information.

Dynamic Explicit Analysis and Prediction of Compressive Damage effects & Stress-strain response of nine Shaft Lining Composites

Bénédicte TOUOGAM TOUOLAK (architekktbenedikkte@gmail.com)
Anhui University of Science and Technology https://orcid.org/0000-0001-8838-355X

Research Article

Keywords: Shaft of coal mines, Engineering application, Explicit finite element analysis (FEA), 3D detailed modelling

Posted Date: March 17th, 2022

DOI: https://doi.org/10.21203/rs.3.rs-1436955/v1

License: This work is licensed under a Creative Commons Attribution 4.0 International License.
Read Full License

Dynamic Explicit Analysis and Prediction of Compressive Damage effects & Stress-strain response of nine Shaft Lining Composites

Bénédicte Touogam Touolak[1, 2]

1 School of Civil Engineering and Architecture, Anhui University of Science and Technology, Huainan 232001, China

2 Department of Civil Engineering and Architecture, National Advanced School of Engineering, University of Maroua, Maroua, Cameroon

Corresponding author: - architekktbenedikkte@gmail.com

Abstract:

In this paper, the nonlinear finite element analysis by ABAQUS was used to predict the behavior and ultimate capacity of shaft lining steel-concrete composite structures. The numerical data for designing the shaft lining structure in coal mines; the stress-strain response and damage of steel-concrete composites is deeply explore through finite element analysis and analytical methods. The present work studies the influence of thickness-diameter ratio on the shaft lining structures performance by focusing on the stress-strain characteristics, geometry imperfections, damage and deformations occurs inside the materials structure properties. The results from the finite element simulation agree very well with the experimental observations, especially with regard to load-deflection response, crack patterns at different load stages, failure modes and stress-strain mechanisms. All these indicate that the constitutive models used for shaft linings concrete by ABAQUS are able to capture compressive behavior and stress-strain response of the different Z1, Z2, Z3, Z4, Z5, Z6, Z7, Z8, and Z9 specimens. The results show

that the nine models have an acceptable agreement with the experimental results for stress-strain response and progressive damage with high reliability. In this paper the traditional bearing capacity calculation formula is also used to calculate the ultimate bearing capacity of the shaft lining structures. The finite element software ABAQUS is employed for modeling, analyzing and simulation of a new high strength composite for coal mining application design. Finally, the plastic strain, compressive damage variable, tensile damage variable, compressive stress-strain curves, and load-displacement diagrams are obtained at the same time verified by incremental loading method employed on ABAQUS for solving the rationality of the shaft lining structures bearing in finite element dynamic analysis.

Based on the present research, for the studied cases, the experiment results of shaft linings concrete and FEM analysis by ABAQUS were in good agreement; the mean ratios of experimental-to-predicted values for: ultimate load capacities equal to 40 MPa; the limit loop strain of steel and concrete varying between 4000 to 6000 $\mu\varepsilon$; the limit loop stress of steel is about 300 to 400 MPa, while for the concrete is about 150 to 200 MPa. Finite element analysis and experimental results show that, as loading progressed, the strain distribution in the shaft lining structure became approximately uniform indicating the formation of a tied arch mechanism. Concrete strain distribution is nonlinear and non-conform to Bernoulli's assumptions for strain and stress distribution; this nonlinearity is due to the shear deformations inside the structural element. The study can provide certain reference for practical engineering calculation and analysis of compressive damage effects & stress-strain response of shaft lining structures.

Keywords: Shaft of coal mines; Engineering application; Explicit finite element analysis (FEA); 3D detailed modelling.

1. Introduction

The development of computer methods for the solution of scientific and engineering problems governed by the laws of mechanics and civil engineering was one of the great scientific and engineering achievements of the second half of the 20th century, with a profound impact on science and technology. Computer technology and finite element theory through the commercial finite element software is growing very fast in most of the international research centers. ABAQUS is one of the large and worldwide use software in the field of structural engineering design and mechanics engineering, also in the field of civil engineering for the structural coal mining design projects. Commonly use in research works and engineering, ABAQUS have a high speed, high accuracy coupling with the low cost analysis of numerical calculations of finite element analysis software. The operator interface of ABAQUS is more convivial than others finite element software and thus, the results visualization is pretty more attractive, especially in the case of explicit analysis with some deformations, shear stress and bending of the structure **[42-68]**.

Computer Methods in Applied Mechanics and Engineering was founded over three decades ago, providing important research data in the field of science and engineering. The range of appropriate contributions is very wide and covers any type of computational method for the simulation of complex physical problems leading to the analysis and design of structural engineering systems. This includes theoretical development and rational applications of mathematical models, variational formulations, and numerical algorithms related to finite element, boundary element, finite difference, finite volume, and meshless discretization methods in diverse fields of computational science and engineering (Solid and structural mechanics, Fluid mechanics, Mechanics of material, Heat transfer, Dynamics, Geomechanics, Acoustics, Biomechanics, Nano mechanics,

Molecular dynamics, Quantum mechanics, Electromagnetics) **[42-68]**. The obtained simulated results coupling with analytical results are compared with the experimental data; an analysis with a discussion of these results are made in order to serve as a reference for further studies of the finite element analysis on ABAQUS.

2. Establishment of the Model

The nine studied shaft lining cylinders are investigated using the ABAQUS FEA package **[56]**. For each parametric configuration two models are solved; one with a Frequency step and one with an Explicit Dynamic step to avoid convergence on calculations.

The model for double steel plate concrete shaft lining is illustrated in Figure 1.

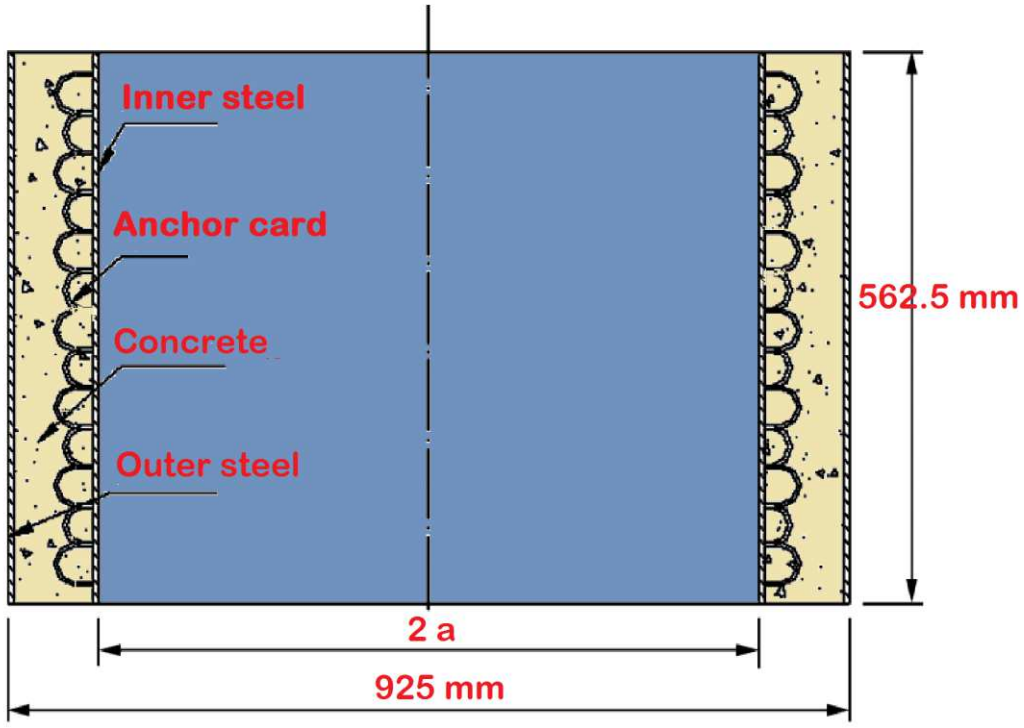

Figure 1: Shaft lining structure model

The steel anchor in the concrete is used to measure the stress, strain, and displacement of the studied structure. For an explicit dynamics analysis the time is an important parameter for the real time data collecting. There is the full-scale shaft lining dimensions, inner and outer thickness, also specimen's concrete strength grade. The height and width of the anchor are half the thickness of the shaft lining model.

2.1 Parameters of Constitutive Model

The ABAQUS element library provides a complete geometric modelling capability. For this reason any combination of elements can be used to make up the model. All elements use numerical integration to allow complete generality in material behavior. Element properties can be defined as general section behaviors, or each cross-section of the element can be integrated numerically, so that nonlinear response can be tracked accurately when needed.

The shaft lining materials are super strength concrete and steel plate applied in both engineering design constructions projects. These materials gives a complete stress-strain curve of strength and load of the composite structure. For the numerical analysis a geometrical ratio dimensions of the shaft lining structure model is adopted, since the prototype dimensions are relatively large.

Because of the investigation of the stress-strain distribution of the shaft lining structure, it will be necessary to evaluate the ultimate loading of the damage. The equations analysis methods of the shaft lining static model is as follows: $\boldsymbol{C_\varepsilon C_l / C_\delta = 1}$ is related to the structure geometry; $\boldsymbol{C_\rho / C_\sigma = 1}$ is a boundary equation; the physical equation of the model is get by:

$\frac{C_\varepsilon C_E}{C_\sigma} = 1, C_v = 1$; where C_l is the geometrical similarity constant, C_ρ the load or surface force similarity constant, C_ε the strain similarity constant, C_E the elastic modulus similarity constant, C_δ the displacement similarity constant, C_σ the stress similarity constant, C_v the Poisson ratio similarity constant. Before and after the loading deformation the shaft lining model will keep the same geometry conditions as show in the follow equation:

$$C_E = C_\sigma = C_\rho = C_R = 1, C_\varepsilon = 1$$

Where C_R is the strength similarity constant, while the bearing capacity is the model ability to bear load. We will consider C_l as the amplified displacement of the model, so we can only approximate the geometrical similarity constant of the shaft lining structure. We consider the elastic strain modulus as the ratio between 40% of load for the axial compressive strength. The Poisson's ratio is uniformly take at 0.2 or 0.26.

2.2 Finite Element Analysis Approach

Finite Element Method (FEM) is a very strict numerical analysis method of theoretical system which converts ideally the continuum into a discrete structure; the structure is composed of a finite number of units and analyzes the stress and deformation according to each unit. The FEM is more comprehensive considering the constitutive relation, strain compatibility condition and static equilibrium between stress and strain; also there are some advantages of solving various complex boundary conditions, heterogeneous and nonlinear structural engineering problems.

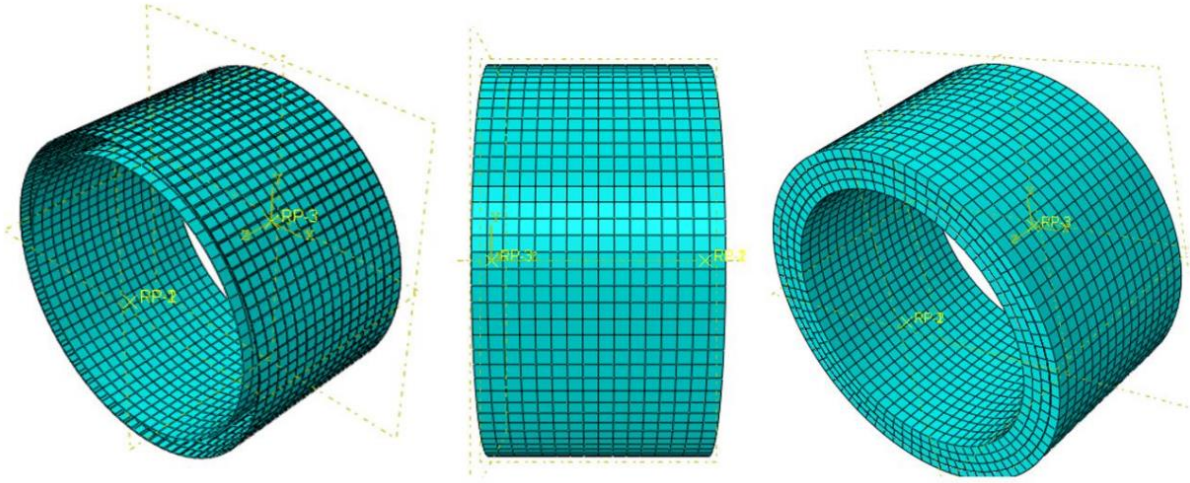

Figure 2: Finite element modelling, geometry and mesh of the shaft lining models

The geometry for the shaft lining model was created using ABAQUS/CAE. The Figure 2 shows the finite element meshes used in the dynamic explicit simulation of a shaft lining borehole cylinder. Reduced-integration shell elements employing stiffness hourglass control have been used to discretize the nine studied composite models. The constitutive behavior of the double steel plate is represented by a rate-dependent Mises plasticity model. The mesh-independent fasteners have also been used to simplify the modeling of parts structure; so the mesh configuration is more smoothly. Surfaces specified in the general contact domain can include rigid and deformable regions with mixed element types. The general algorithm enforces constraints using a specific method which works very well with mesh-independent fasteners, and other type of constraints.

Several researchers have carried out numerical simulation and finite element modeling of concrete structures. It was found that the FEM is in good agreement with the experimental tests data. The general contact algorithm in ABAQUS/Explicit is used for this analysis. The design of shaft lining model parameters consider the ultimate thickness which have been previously studied in the reference **[1]** during the experimental tests. The inner and outer cylinder thickness will vary according to the height of each models. The three steel-

concrete composites C65, C70 and C75 are considered in this research paper according to the "Code for Design of Concrete Structures" **[36-38]**.

2.3 General Methodology: Model geometry, Boundary conditions, and Loading

Numerical simulations of shaft linings composites were done by using commercial software ABAQUS Standard 6.12 **[56]**. The concrete material was modelled as a homogeneous 3D solid section; the Drucker-Prager plasticity model is used during the numerical simulation of the composite. The numerical model should be able of capturing the critical and essential phenomena which occurs inside the material structure **[20-35]**.

The axial and tangential axes are constrained along the circumference. The cylinder bottom is encastred with pinned conditions, while the top cylinder is subject to peak deformations. All the steel cylinders of the composite are fixed at the bottom, and the top end is kept free in all directions with the applied axial loading. Embedded region constraint available in ABAQUS Standard is used to define the bonding of steel-concrete composite. To determine the axial load-deflection history of shaft lining structures up to failure, a static monotonic load is applied at the top by the displacement control. The constraint tie is used to apply the boundary conditions and an equal distribution of different loads. The steel plates are considered as rigid elements with Young's modulus of 210 GPa and density of $7.85.10^{-9}$ ton/mm^3. The most specific details of the geometry and modelling finite element models of shaft lining composites are shown in Figure 2.

3. Model Test Verification

3.1 Details of validated model

The solid (or continuum) elements in ABAQUS can be used for linear analysis and for complex nonlinear analyses involving contact, plasticity, and large deformations. In this research paper, regarding the finite element models, three dimensional 8-node first order fully integration continuum elements (C3D8 – Bricks) are used to model the concrete composites and loading steel plate's cylinders. The mentioned abbreviation stands for:

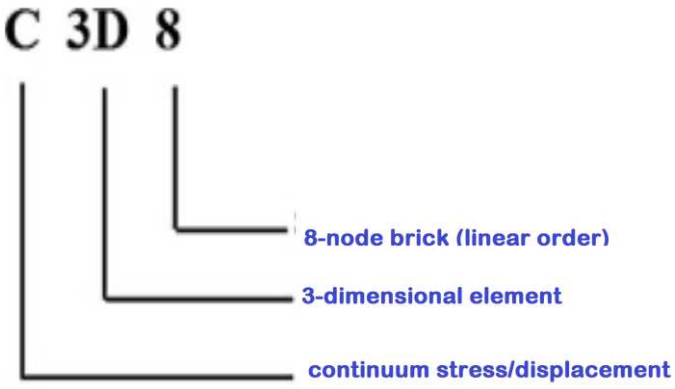

Most of the time the geometry size of the cylinders models is not helpful for the full-experimental tests; in the case of numerical analysis a reduced-scale model is consider during the input parameters in the finite element software ABAQUS. The outside diameter of the model is 925 mm while the height is 562.5 mm (see Figure 1). For the shaft lining thickness-diameter ratio we have the values of 0.2692 mm, 0.2886 mm, and 0.3076 mm for 98.1 mm, 103.6 mm, and 108.8 mm respectively.

Because of the elasticity of the studied models we consider the equilibrium, geometric and physical equations which take in account the strain ratio, displacement, force, stress and Poisson ratios. Several expressions should be consider as shown below:

$$\frac{C_{\varepsilon}.C_l}{C_u} = 1 \quad (1)$$

$$\frac{C_{\vec{X}}}{C_{\sigma}} = 1 \quad (2)$$

$$\frac{C_{\varepsilon}.C_E}{C_{\sigma}} = 1, C_v = 1 \quad (3)$$

Where C_{ε} is the strain similarity ratio, C_l the geometry similarity, C_u the displacement ratio, C_E the elasticity modulus ratio and C_v the Poisson's ratio. These initial conditions are important to satisfied and ensure the strain relationship between the full-scale shaft lining and the nine different studied models. In this case $C_{\varepsilon} = 1$ and the previous equations 1, 2, and 3 can be simplified in the equation 4 below:

$$\frac{C_l}{C_u} = 1, \frac{C_{\vec{X}}}{C_{\sigma}} = 1, \frac{C_E}{C_{\sigma}} = 1, C_v = 1 \quad (4)$$

The strength conditions have to be satisfied to ensure a good deal between the failure load and the failure form of the nine shaft lining models. Those equations are helpful to get the stress-strain relationship point of the models during the loading process. The failure criterion and the strength part of the model are important for the stress-strain characteristics. All the models materials are similar and satisfied the strength also boundaries conditions as specified in the equation 5.

$$C_l = C_u, C_E = C_v = C_{\sigma} = C_{\vec{X}} = C_{\rho} = C_f = 1 \quad (5)$$

The steel content here is symbolize by C_ρ, while the strength similarity ratio is materialize by C_f.

3.2 Reasonability of numerical model

The FE models are generated using ABAQUS CAE FE package and the models are parameterized via Python scripts. In order to apply the loads and boundary conditions (BCs), a reference point is set at the center of each free edge of the cylindrical shells and connected using multi-point constraint (MPC). Also to obtain accurate results from the FE model, all the elements in the model were purposely assigned the same mesh size to ensure that each of two different materials shares the same node. The type of mesh selected in the model is structured; modeling and mesh generation are developed using same techniques for all specimens.

The nine studied models are composed of two materials: steel and concrete. When the concrete is undergoing elastic deformations, the circumferential stresses are distributed according to the stress distribution law of thick-wall cylinders defined by:

$$\boldsymbol{\sigma_t = \frac{b^2\rho}{b^2-a^2}\left(1+\frac{a^2}{r^2}\right)} \qquad \textit{(6)}$$

Where σ_t is stress circumference of the concrete; ρ the external load; a is the inner radius and b the outer radius of the shaft lining structure; r is the radius at the calculation point in the finite element software.

For the comprehensive physical and mechanical properties of the nine studied shaft lining composites we can refers to the Table 1. The modulus of elasticity (E_c) of concrete was calculated using the ACI code given by the following expression:

$$E_c = 4700\sqrt{f_c^l} \qquad (7)$$

Table 1: Physic-mechanical parameters of shaft lining structures

N°	Concrete Strength Grade/MPa	Thickness-Diameter Ratio	Concrete Compressive Strength/MPa **[1]**	Ultimate Strength/MPa **[1]**	**Analytical data (MPa)**		
					Strain at end of softening curve	Elastic Modulus/MPa	Poisson's ratio
Z1	C60	0.2692	66.9	29.5	0.0039	23.020	0.2
Z2	C60	0.2692	71.1	33	0.0040	22.850	0.2
Z3	C60	0.2692	75.6	37	0.0040	24.150	0.2
Z4	C70	0.2886	65.8	33.5	0.0040	22.450	0.2
Z5	C70	0.2886	71.4	38	0.0038	23.320	0.2
Z6	C70	0.2886	76.5	37.5	0.0031	23.210	0.2
Z7	C80	0.3076	65.8	36	0.0030	23.680	0.2
Z8	C80	0.3076	71.5	35	0.0042	24.290	0.2
Z9	C80	0.3076	76.8	40	0.0036	24.140	0.2

The master and slave surface concept was used to define the interaction between concrete cylinders and steel plates. The bottom surface of the top steel plate and the bottom surface of the concrete cylinder was taken as master's surfaces; the top surface of the concrete cylinder and the top surface of the bottom steel plate are considered as slave's surfaces. The load transferring surfaces are taken as master surfaces.

A total of 09 full-scale cylinders specimens were modelled in ABAQUS under different loading conditions, from which all the 09 specimens were reinforced longitudinally and transversely with thin steel cylinders (the thin steel cylinders have different diameter ratio according to their inner and outer diameter thickness).

4. Parameters analysis

4.1 Simulation Scheme

The numerical simulation will be conducted by using the Python code on the Commercial Finite Element Software ABAQUS **[56]**. The stress-strain relationship is obtain during the deformation when the material tend to stabilize; the ultimate bearing can also be observe at this stage until failure when the loads are applied.

4.1.1 Stress invariants

The yield stress surface makes use of two invariants, defined as the equivalent pressure stress,

$$\boldsymbol{\rho = -\frac{1}{3}\, trace\,(\sigma);} \qquad \textit{(8)}$$

And the Mises equivalent stress,

$$\boldsymbol{q = \sqrt{\frac{3}{2}}\,(S : S);} \qquad \textit{(9)}$$

Where S is the stress deviator, defined as:

$$\boldsymbol{S = \sigma + \rho I} \qquad \textit{(10)}$$

In addition, the linear model also use the third invariant of deviatory stress,

$$\boldsymbol{r = (\frac{9}{2}\, S\,.S\,.S)1^{\frac{1}{3}}} \qquad \textit{(11)}$$

4.1.2 Yield stress ratios

Alternatively, the strain rate behavior can be assumed to be separable, so the stress-strain dependence is similar at all strain rates:

$$\bar{\sigma} = \sigma^0 \left(\overline{\varepsilon^{pl}}\,, \theta\,, f_i\right) R\left(\dot{\varepsilon}^{pl}\,, \theta\,, f_i\right), \qquad \textit{(12)}$$

Where $\sigma^0 \left(\overline{\varepsilon^{pl}}\,, \theta\,, f_i\right)$ is the static stress-strain behavior and $R\left(\dot{\varepsilon}^{pl}\,, \theta\,, f_i\right)$ is the ratio of the yield stress at nonzero strain rate to the static yield stress. Two methods are offered to define R in ABAQUS; specifying an overstress power law or defining the variable R directly as a tabular function of $\dot{\varepsilon}^{pl}$

The Cowper-Symonds overstress power law has the form:

$$\dot{\varepsilon}^{pl} = D\,(R-1)^n \;\; For \;\; \bar{\sigma} \geq \sigma^0\,, \qquad \textit{(13)}$$

Where $D\ (\theta\ ;\ f_i\ )$ and $n\ (\ \theta\ ,f_i\ )$ are material parameters that can be functions of temperature and, possibly, of other predefined field variables.

4.1.3 Linear Drucker-Prager model

The linear model is written in terms of all three stress invariants. It provides for a possibly noncircular yield surface in the deviatory plane to match different yield values in triaxle tension and compression, associated inelastic flow in the deviatory plane, and separate dilation also friction angles.

The linear Drucker-Prager criterion is written as **[30-41]**:

$$\boldsymbol{F = t - p\,tan\beta - d\ =\ 0,} \qquad \textit{(14)}$$

Where;

$$\boldsymbol{t\ =\ \frac{1}{2}\,q\,[1+\frac{1}{K}-\left(1-\ \frac{1}{K}\right)\ (\frac{r}{q})^{3}}\ \textit{]} \qquad \textit{(15)}$$

$\boldsymbol{\beta\ (\theta\ ,f_i)}$ is the slope of the linear yield surface in the p-t stress plane and is commonly referred as a friction angle of the material;

$\boldsymbol{d}$ is the cohesion of the material; and $\boldsymbol{K\ (\theta\ ,f_i)}$ is the ratio of the yield stress in triaxial tension to the yield stress in triaxial compression and, thus, controls the dependence of the yield surface on the value of the intermediate principal stress as show in the Figure 3.

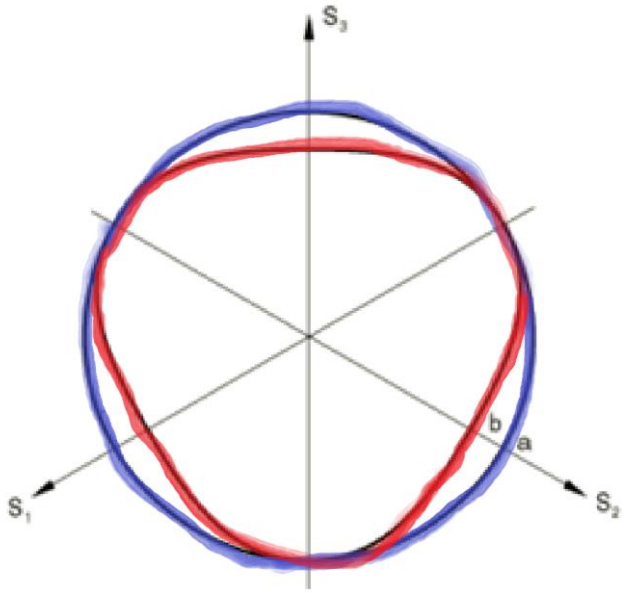

Figure 3: Yield flow surfaces of the linear model in the deviatory plane

$$\boldsymbol{t = \frac{1}{2} q \left[1 + \frac{1}{K} - \left(1 - \frac{1}{K}\right)\left(\frac{r}{q}\right)^3\right]} \qquad (16)$$

***Table 2*: Linear yield criterion**

Curve	**K**
a	1.0
b	0.8

For the hardening defined in uniaxial compression, the linear yield criterion precludes friction angles $\boldsymbol{\beta > 71.5°}$ $\boldsymbol{(tan\beta > 3)}$, which is unlikely to be a limitation for real materials.

When $\boldsymbol{K = 1, t = q}$, which implies that the yield surface is the von Mises circle in the deviatory principal stress plane; in which case the yield stresses in triaxle tension and compression are the same. For a convex yield surface we need to make sure that the following expression 17 is verified:

$$\mathbf{0.778} \leq \boldsymbol{K} \leq \mathbf{1.0} \qquad \textit{(17)}$$

The cohesion d of the material is related to the input data as:

$\boldsymbol{d} = \left(\mathbf{1} - \frac{\mathbf{1}}{\mathbf{3}}\mathbf{tan}\,\boldsymbol{\beta}\right)\boldsymbol{\sigma_c}$ if the hardening is defined by the uniaxial compression yield stress, σ_c;

$= \left(\frac{1}{K} + \frac{1}{3}\tan\beta\right)\sigma_t$ if hardening is defined by the uniaxial tension yield stress, σ_t;

$= d$ if the hardening is defined by the cohesion, $d = \frac{\sqrt{3}}{2}\,\tau\,(1 + \frac{1}{K})$

4.2 Verification of the Empirical Formula for the Ultimate Capacity

The numerical model is built in ABAQUS CDP (Concrete Damage Plasticity) model based on the concrete stress-strain curve provided by the code FORTRAN for concrete structure design. The key of finite element method to solve the ultimate bearing capacity is how to determine whether the structure reaches the ultimate destructive state based on the results of finite element calculation. There are several criteria **[39-68]** as follows:

The first criteria is according to the finite element calculation and the convergence which is the standard for the failure of shaft lining structures. The corresponding load to the non-convergence is taken as the ultimate bearing capacity of the structure. During the structure instability, the displacement and plastic strain can mutate so the numerical calculation won't converge.

For the second criteria, the plastic area on the structure reflect the damage state and take the corresponding load during the ultimate bearing capacity of the shaft lining. There is a possibility to map the distribution of generalized plastic strain at this step.

The third criterion is the ultimate load which correspond here to the inflection point on the displacement (s) and load (p) curve. The displacement and load curve of the FEM are the most intuitive reaction of the shaft lining structure instability. The inflection point of the p-s curve is used as a criterion of critical damage state of the structure.

Table 3: Parameters and capacities of shaft lining models

N°	Concrete Strength Grade/MPa	Thickness-Diameter Ratio	Concrete Strength (MPa)	**Ultimate Capacity /MPa**		
				Test Value /MPa	Calculated Value /MPa	Relative Error /%
Z1	C60	0.2692	66.9	29.5	27,97	1.41
Z2	C60	0.2692	71.1	33	31,34	1.38
Z3	C60	0.2692	75.6	37	35,18	1.64
Z4	C70	0.2886	65.8	33.5	31,74	1.55
Z5	C70	0.2886	71.4	38	36,1	1.87
Z6	C70	0.2886	76.5	37.5	35,81	1.73
Z7	C80	0.3076	65.8	36	34,18	2.02
Z8	C80	0.3076	71.5	35	33,45	1.49
Z9	C80	0.3076	76.8	40	38,28	1.77

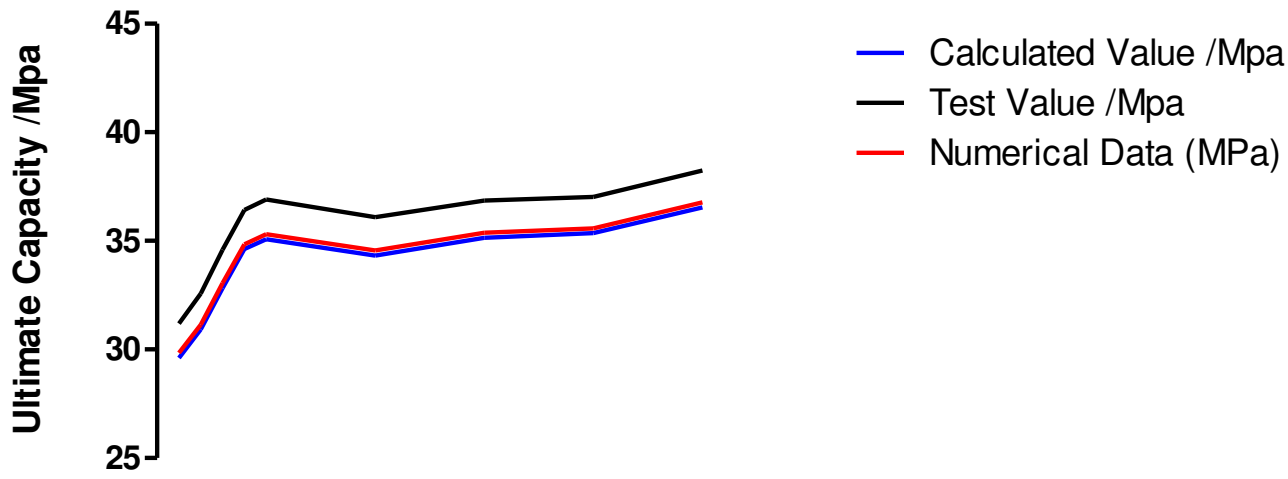

Figure 4: Comparison curves of ultimate bearing capacity of shaft lining structures

At the ultimate load state, the compressive strain distribution in the concrete is nonlinear as it no longer follows the parabolic shape or intensity linearity of normal (shallow) shaft linings. This condition is due to the predominant effect of the post-cracking, the reduction in the concrete's compression area and the shear deformation that is prevalent in shaft linings structures.

4.3 Progressive damage and failure

The damaged plasticity model for concrete available in the ABAQUS material library is adopted to model concrete response, since it has been shown to perform satisfactorily in similar applications **[2-19]**. In ABAQUS/Explicit the extended Drucker-Prager models can be used in conjunction with the models of progressive damage and failure. The ability allows for the specification of one or more damage initiation criteria, including ductile, shear, forming limit diagram (FLD), forming limit stress diagram (FLSD), and Müschenborn-Sonne forming limit diagram

(MSFLD) criteria. After damage initiation, the material stiffness is degraded progressively according to the specified damage evolution response. The model offers two failure choices, including the removal of elements from the mesh as a result of tearing or ripping of the structure. The progressive damage models allow for a smooth degradation of the material stiffness, making them suitable for both quasi-static and dynamics situations **[30-41]**.

Table 4: Damage parameters data before failure

N°	Concrete Strength Grade/MPa	Thickness-Diameter Ratio	Concrete Compressive Strength/MPa **[1]**	Ultimate Strength/MPa **[1]**	**Numerical Simulation data (MPa)**	
					Axial Compressive Strength	Ultimate Capacity /MPa
Z1	C60	0.2692	66.9	29.5	65.82	28,2
Z2	C60	0.2692	71.1	33	70.73	31,57
Z3	C60	0.2692	75.6	37	73.11	35,41
Z4	C70	0.2886	65.8	33.5	66.2	31,97
Z5	C70	0.2886	71.4	38	69.42	36,33
Z6	C70	0.2886	76.5	37.5	75.35	36,04
Z7	C80	0.3076	65.8	36	65.4	34,41
Z8	C80	0.3076	71.5	35	71.14	33,68
Z9	C80	0.3076	76.8	40	75.78	38,51

In case where the specimen failed in shear-compression (SC), the load decreased abruptly upon reaching the ultimate value and failure was brittle. But for specimens that failed in flexure (FC), the load remained almost constant with increasing deflection at ultimate, indicating ductile specimen behavior. Generally, the cracks propagated toward the loading point as the load is increasing; we can observe more flexural-shear cracks along the shaft lining shear spans. So there will be an eventual shear-compression failure resulting in the crushing of concrete in the compression zone of the shaft lining structure. ABAQUS can monitor and

capture the shape and propagation of cracks during loading till failure **[20-56]** as show in the Figure 5.

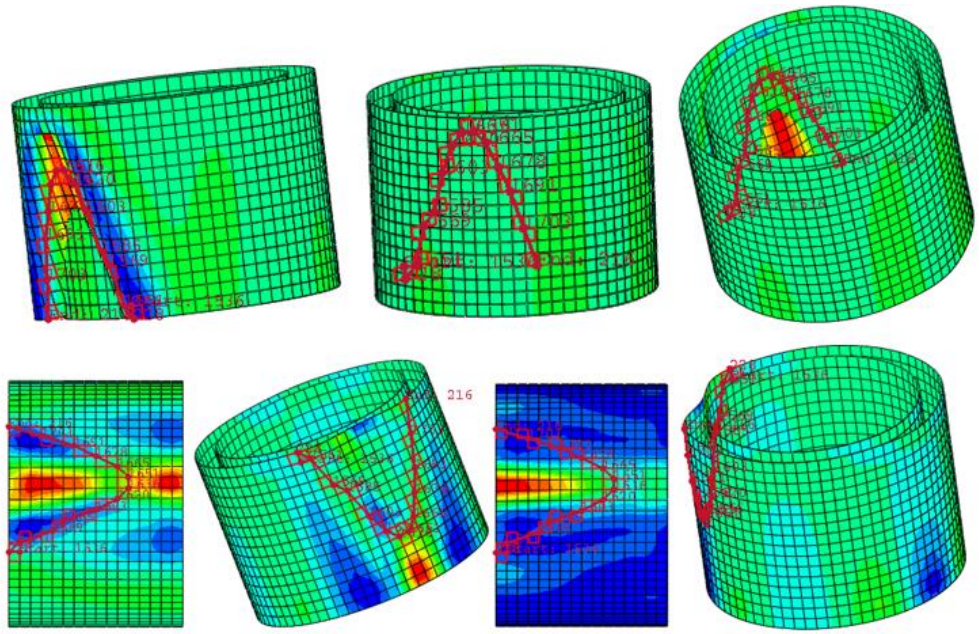

Figure 5: Shape and propagation of cracks during loading till failure of the Shaft Lining Structure

The strain distribution along the bottom layer of the borehole cylinder as the load increased is shown in Figure 5; as more cracks formed closer to the supports, the measured strains in the composite model would also increase closer to the support. In the un-cracked regions, strain readings showed minimal strain changes in the shaft lining composite structure. As loading progressed, the strains in the structure became similar between the supports indicating the formation of a tied arch mechanism **[2-19]**.

4.3.1 Definition of plastic flow potential and yield function

Concrete is a complex material characterized by several parameters as compressive strength, tension strength, crushing energy, fracture energy, and many others structural parameters **[20-41]**. The most important characteristics can be calculated directly from the average strength f_{cm} which can be obtained through the static uniaxial compressive experiments. From this parameter it is more convenient to establish the CDP (Concrete Damage Plasticity), and to describe the concrete behavior from the un-crack / un-crush stage to the failure stage. The CDP model is widely used in ABAQUS software to increase the concrete strength due to the effects of confinement **[56]**.

According to the CDP model, the following non-associated potential plastic flow rule is used:

$$\dot{\varepsilon_p} = \dot{\lambda} \frac{\partial G}{\partial \sigma} \qquad (18)$$

Where σ and $\dot{\varepsilon_p}$ denote the stress and plastic strain rate tensors, respectively, $\dot{\lambda}$ is a plastic multiplier and G defines Drucker-Prager hyperbolic function in the model given by the equations 19 and 20.

$$G = \sqrt{(\in \sigma_{to} \tan\phi)^2 + (\overline{q})^2} - \bar{p} \tan\psi \qquad (19)$$

$$\bar{p} = -\frac{1}{3} tr\,(\sigma)\,,\ \bar{q} = \sqrt{\frac{3}{2}}\,\|dev(\sigma)\| \qquad (20)$$

Where $\bar{p}$ and $\bar{q}$ are the hydrostatic stress and the von-Mises equivalent stress, respectively. The parameter ψ is the dilation angle registered in the $\bar{p} - \bar{q}$ plane at high confining pressure. $\in$ Denotes the eccentricity of the potential plastic surface, which is defined as the rate at which the function reaches the uniaxial tensile.

The default value used in ABAQUS is equal to $\in = 0.1$ and the uniaxial tensile stress at failure condition is σ_{to}.

The yield surface of the concrete have the coefficient $\frac{\sigma_{bo}}{\sigma_{co}} = 1.16$

This coefficient causes the compressive stress to increase due to the effective confinement and it can be obtained from the maximum of the experimental range, including a uniaxial and biaxial compression test.

However, this coefficient is only suitable to simulate problems which are affected by the normal strength. On the case of a composite shaft lining concrete-steel, this coefficient is modified based on experimental studies and a ratio of a biaxial-to-uniaxial compressive strength **[39-77]**. Especially, in this research paper, we propose $\frac{\sigma_{bo}}{\sigma_{co}} = 1.42$ to establish the yield surfaces of concrete in static and dynamic loading for compressive high-strength shaft lining concrete.

4.3.2 Compressive behavior

For the concrete especially, it is characterized by the stress-strain relationship. Thus, if the stress is between 0 and $0.4 f_{cm}$, the stress-strain relationship is linear,

and if the stress is between $0.4f_{cm}$ to f_{cm}, the stress-strain relationship is nonlinear. After reaching the peak value f_{cm}, the compressive damage variable d_c is used for the strain at equivalent compression plastic ε_c^{pl}, and elastic ε_c^{el}. The crushing strain ε_c^{in} denotes the damaged extent of concrete in compression loading. For this research paper we will focused on the three principal phases of the concrete behavior as shown below **[19-41]**:

Phase 1:

The stress and strain relationship of the concrete has a linear relationship, and the stress-strain relationship is expressed as follows:

$$\sigma_c^1 = E_0 \varepsilon_c \qquad (21)$$

This linear relationship can be determined based on the secant modulus of concrete materials, which is determined by equations 22 and 23:

$$E_0 = \left(0.8 + 0.2\frac{f_{cm}}{88}\right) E_{ci} \qquad (22)$$

$$E_{ci} = 10000 f_{cm}^{1/3} \qquad (23)$$

Phase 2:

Here the concrete reaches the crushing strain, and the stress-strain relationship is nonlinear and determined by the following equation 24:

$$\sigma_c^2 = \frac{E_{ci}\frac{\varepsilon_c}{f_{cm}} - \left(\frac{\varepsilon_c}{\varepsilon_{ctm}}\right)^2}{1 + \left(E_{ci}\frac{\varepsilon_c}{f_{cm}} - 2\right)\frac{\varepsilon_c}{\varepsilon_{ctm}}} f_{cm} \qquad (24)$$

Where E_{ci} is the Modulus of concrete's elasticity

Phase 3:

In this phase, the concrete stiffness starts to decrease due to the appearance of d_c, and the stress-strain relationship can be calculated by using the equation 25.

$$\sigma_c^3 = f_{cm} + \left(\sigma_f - f_{cm}\right) exp\left[\zeta\left(1 - \frac{\varepsilon_f - \varepsilon_{cm}}{\varepsilon - \varepsilon_{cm}}\right)\right] \qquad (25)$$

Where σ_f, ε_f are the stress and strain at the complete crushing. For this research paper we consider $\sigma_f = 0.7 f_{cm}$ and the parameter ζ also ε_f are not obtained from experimental data; their values are proposed to match the numerical data and experiments. We should remember that the values of ζ and ε_f are only useful for the high concrete grades as C65, C70, C75. The stress-strain relationship of the nine studied shaft lining models are presented in the Figures 8, 9, 10, and 11.

4.3.3 Compressive damage variable

This parameter is used to define the compression hardening data for the concrete damaged plasticity material model. It can also be used to specify the compressive stiffness degradation. Noted (d_c), this parameter assumed that damage initiates only after the maximum stress is attained, because it is very challenging to get the damage quantitatively during the compression test **[39-77]**. So the equation 26 is proposed to calculate the compressive damage variable:

$$d_c = 1 - \frac{f}{f_{cm}} \qquad (26)$$

To improve the damage model of concrete it is benefit to consider the effects of mesh size as mentioned in the equation 27.

$$d_c = 1 - \frac{1}{2+a_c}[2(1+a_c)\,exp(-b_c\varepsilon_c^{ch}) - a_c\,exp(-2b_c\,\varepsilon_c^{ch} \qquad (27)$$

Where a_c and b_c can be determined from the equations 28 and 29.

$$a_c = 2\left(\frac{f_{cm}}{f_{co}}\right) - 1 + 2\sqrt{(f\frac{cm}{f\,co})^2} - \sqrt{(f\frac{cm}{f\,co})} \qquad (28)$$

$$b_c = \frac{f_{co}I_{eq}}{G_{ch}}(1 + \frac{a_c}{2}) \qquad (29)$$

Where f_{co} denotes uniaxial compressive yield strength, I_{eq} denotes the mesh size in the numerical model. The Figures 6 and 7 shows the relationship of compressive damage variable-crushing strain of shaft lining models C65, C70, and C75.

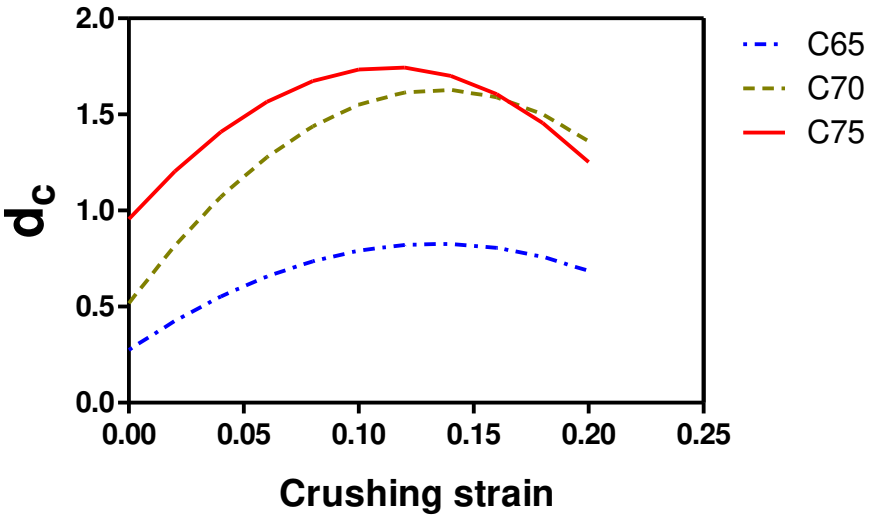

Figure 6: Compressive damage variable (dc) vs. crushing strain

4.3.4 Tensile behavior

At this phase, when the concrete has no cracks, the stress-strain relationship is considered linear and determined through the modulus of elasticity. At this stage of concrete, the behavior is independent of the mesh size after the crack phenomenon, and the strain-softening phase appear when the stress-strain relationship becomes nonlinear and dependent of the finite elements mesh size. When the cracks appear in the concrete, they are growing very fast until the failure of the concrete **[39-77]**. The mesh size l_{eq} in the FEM is responsible of the convergence after the model implementation.

The curve of stress-crack opening to replace the stress-strain curve is given by the equation 30.

$$\frac{\sigma_t(w)}{f_m} = \left[1 + \left(C_1 \frac{w}{w_c}\right)^3\right] e^{-C_2 \frac{w}{w_c}} - \frac{w}{w_c}(1 + c_1^3)e^{-C_2} \qquad (30)$$

Where $C_1 = 3$; $C_2 = 6.87$ and w_c is the critical crack opening; it can be considered as the fracture crack opening according to the equation 31.

$$w_c = 5.14 \frac{G_F}{f_m} \qquad (31)$$

For the numerical analysis of this paper, the crack spacing is ignored because of the mesh size effects. Also, we can observe that the crack occurs in each element after tensile stress reaches a maximum peak. The strain at tensile strength ε_m can be calculated from crack opening by the equation 32.

$$\varepsilon_t = \varepsilon_m + \frac{w}{l_{eq}} \qquad (32)$$

Where l_{eq} is the length of the element mesh or the mesh size. From the obtains results, we deduct that the tensile stress-strain is more suitable when we use the finite element analysis, because it consider the effects of elements length as the mesh size, and also can be calculated from the previous equations 30, 31, and 32.

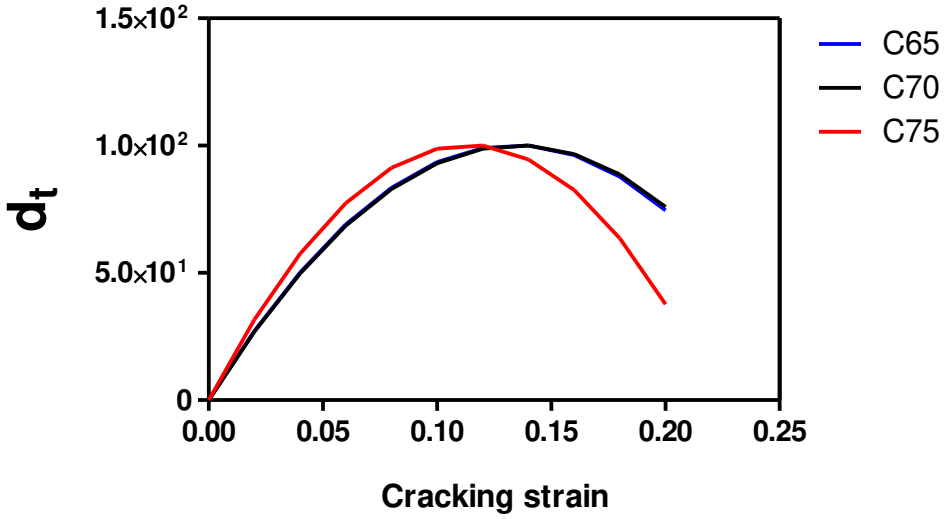

Figure 7: Tensile damage variable (d_t) vs. Cracking strain

4.4 Numerical Simulation Results

4.4.1 High-strength composite shaft linings

The experiments of Reference work **[1]** are used to quantify the average compressive strength in the static and dynamic conditions of concrete composites Z1 to Z9. The specific concrete grades are C65, C70, and C75 with a model structure height varying between 98.1 mm to 108.8mm.

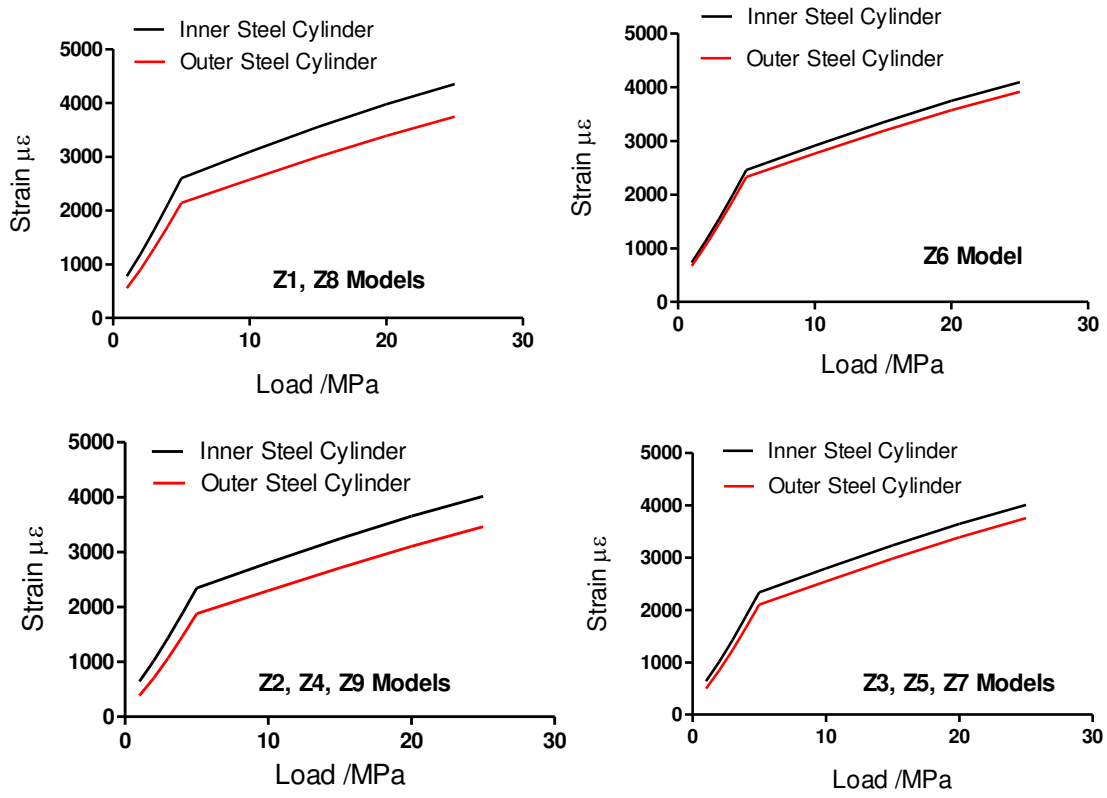

Figure 8: Strain and loading correlation curves between the inner and outer of steel plates for the different shaft lining models

Plots of the strain-stress variations determined by the FE analysis along the section circumference of the cylinder under first crack load and ultimate load are shown in Figures 4, 8, 9, 10, and 11. It shows that the strain-stress distribution in the shaft lining structure is nonlinear. The number of neutral axes decreases with incremental loads and, at ultimate stage only one neutral axis is present. The compression strain in the top circumference cylinder increases as the load increases; but in the tension area, the strain predictions are disturbed by the cracks propagation (see Figure 5).

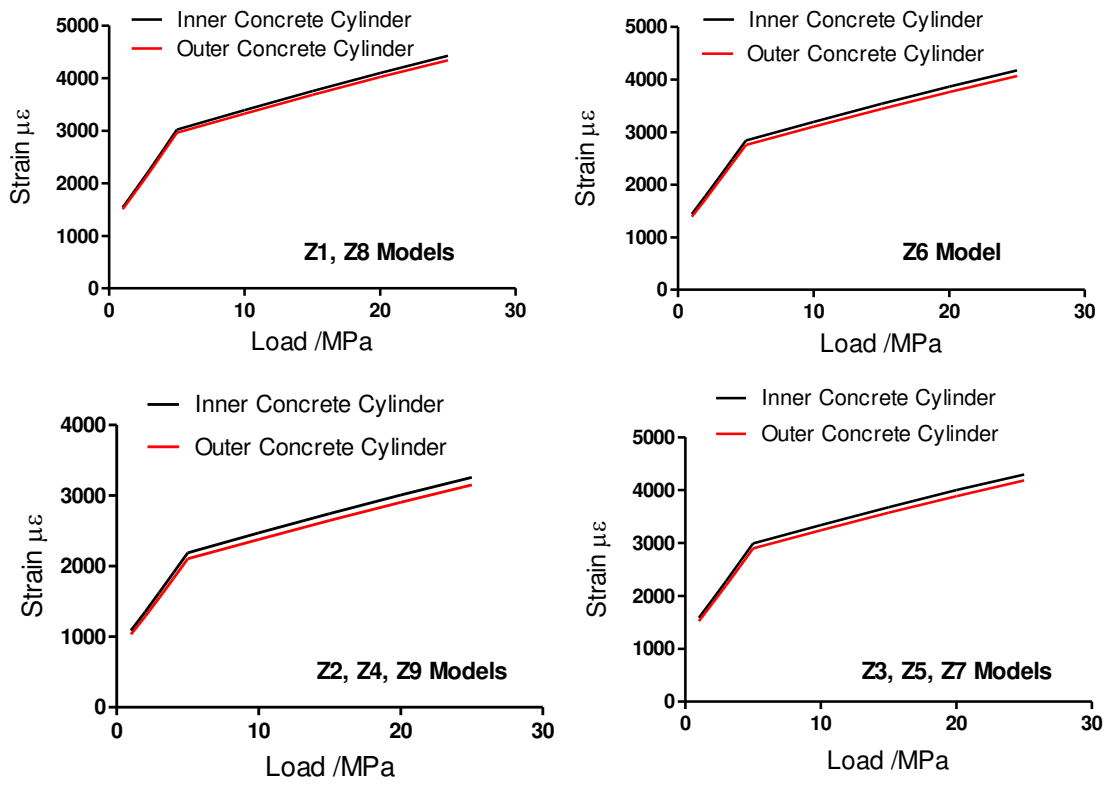

Figure 9: Correlation curves between strain and load of the shaft lining steel-concrete structure, inner and outer ledge for the different models

Distribution of strains along the concrete surface and compression structure were modeled by finite element analysis using ABAQUS, and the various locations of strain gauges to monitor the strains are shown in Figures 8 and 9.

The difference in the maximum compression strain in the extreme compression concrete in shallow and deep shaft linings is due to reasons such as the size effect and the load transferring mechanism; another reason is the concrete strength because the shallower compressive stress model is required to equilibrate the tension zone forces. The stress-strain curves in the Figures 9 and 11 shows the increasing of concrete compressive strength during the static load application under dynamics conditions. The stress-strain relationship curves will be necessary for a further validation of the experimental proposed model of the reference work

[1]. A CPD model is proposed in the next section and verified by the static and dynamics calculations through the Finite Element Software ABAQUS.

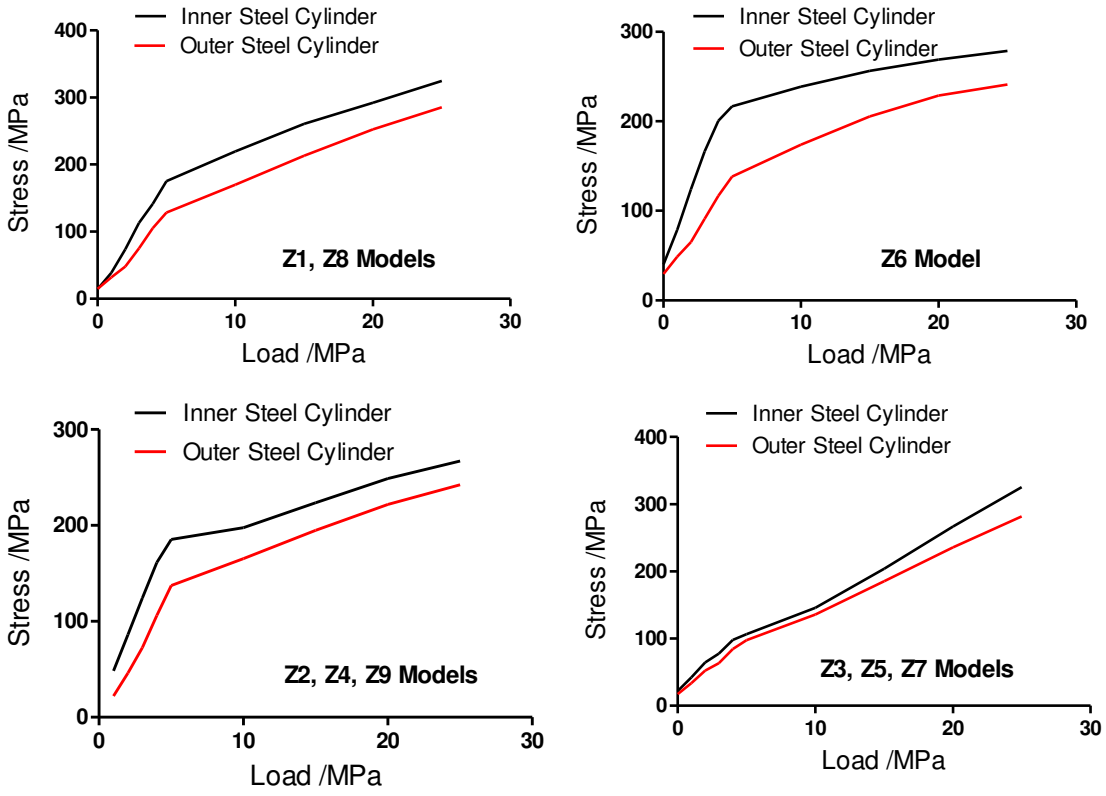

Figure 10: Stress and loading correlation curves between the inner and outer of steel plates for the different shaft lining models

The stress are obtained from the numerical strain values by calculation using the formula of the equations 6, 8, 9, 10, and 11. The load stress curves are plotted in the Figures 10 and 11; it shows that the load hoop stress of the steel and concrete are constrained. For the small loads the shaft lining structure show interesting linear elastic characteristics, and the stress of the nine studied composites increase linearly according to the applied loads. The stress distribution vary considerably and is more complex for the steel-concrete shaft lining; the whole structure is

subject to compressive stress under uniform load. We can observe a high deviation of the stresses values when the concrete structure enter the elastic-plastic stage.

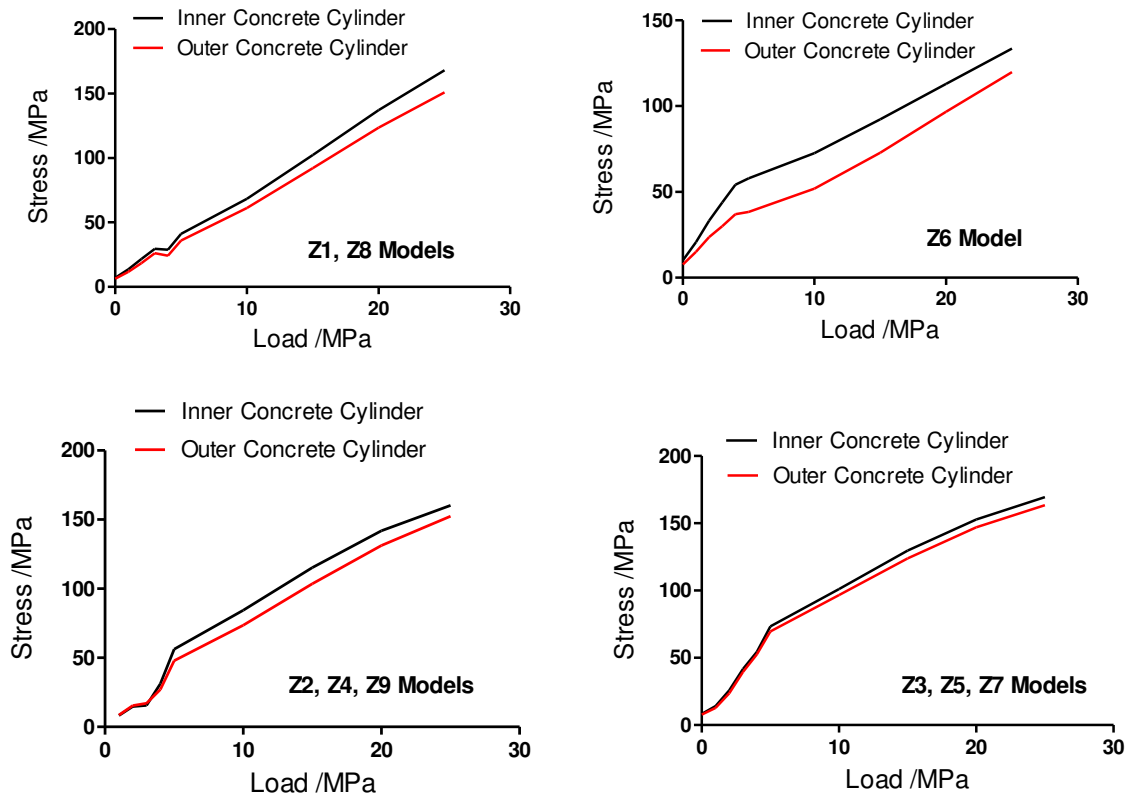

Figure 11: Correlation curves between stress and load of the shaft lining steel-concrete structure, inner and outer ledge for the different models

In the triaxle conditions, the coefficient compressive strength of the concrete increase and there is some stress distributions at the top circumference of shaft lining. The critical value is obtain at the failure load step, which satisfied the stress and deformation conditions. The linear load is observe at the elastic stage of the concrete; the load increase has a direct impact on the strain and plastic stage of the concrete. The large plastic deformation always precede the total destruction of the concrete composite. So it is convenient to conclude that the shaft lining

diameter-ratio considerably affect the bearing capacity of the nine studied composite cylinders.

4.4.2 Discussion Results

The numerical data available in this research paper show the large gap between the strain values of different models (Figures 8, 9, 10, 11). Bernoulli's hypothesis facilitates the flexural design of shaft linings concrete structures by allowing a linear strain distribution. The Figure 12 shows that the shaft lining composite is far from being linearly elastic when the ultimate load is reached. This nonlinearity of strain distribution is due to the shear deformations that are often less obvious in concrete structures, but that are significant in shaft lining steel-concrete composites.

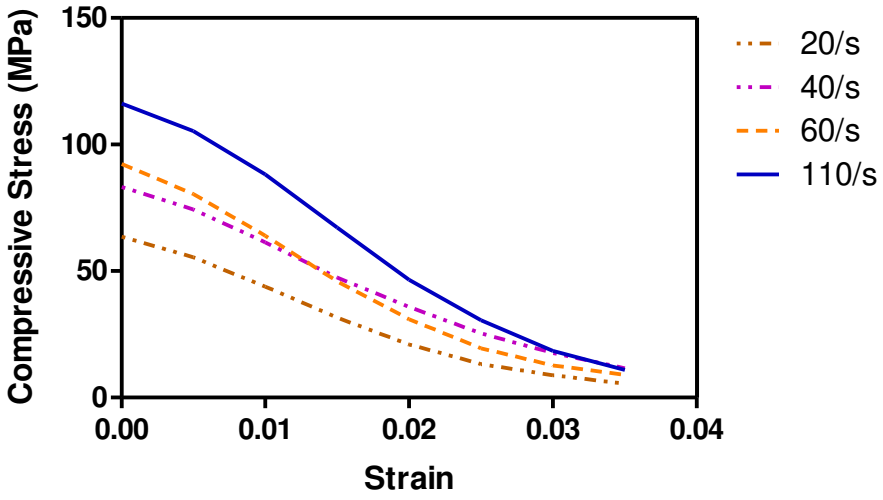

Figure 12: Compressive stress-strain curves of typical concrete C70 under different strain rates

The compressive strains along the shaft lining structure with the highest measured strain are around 0.04. It can also be seen that shaft linings composite exhibit a significant reduction in stiffness after the initiation of the first crack; this behavior is attributed to the low elastic modulus of the steel-plates cylinders. The low modulus of elasticity affects the ability to control concrete cracking. This decreases the tension stiffening effect for concrete between cracks leading to a reduced effective moment of inertia and hence large deflections (see Figure 13).

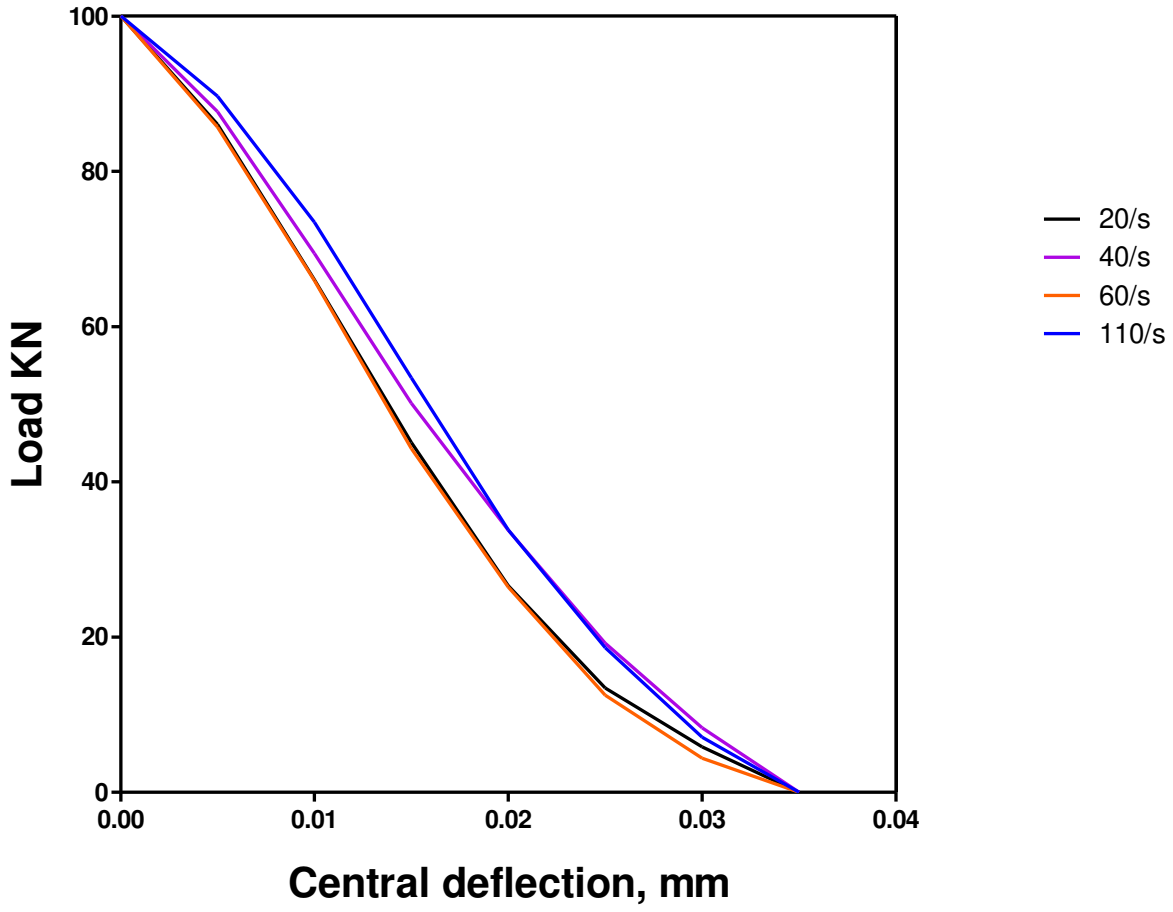

Figure 13: Effect of steel-plates on load-deflection response of shaft linings composite structures

At the initial boundary conditions during the load stage, the hoop strain both of the steel and concrete shaft lining structure still linear according to the load conditions. The change shape of the structure material display with the concrete strength; especially during the elastic stage of the shaft lining. The bearing capacity vary at the ultimate elastic load until the failure of the shaft lining composite.

A linear relationship can be observe between the hoop strain of the steel and the concrete when the applied load increase with time. The steel strain value is much higher than for the concrete.

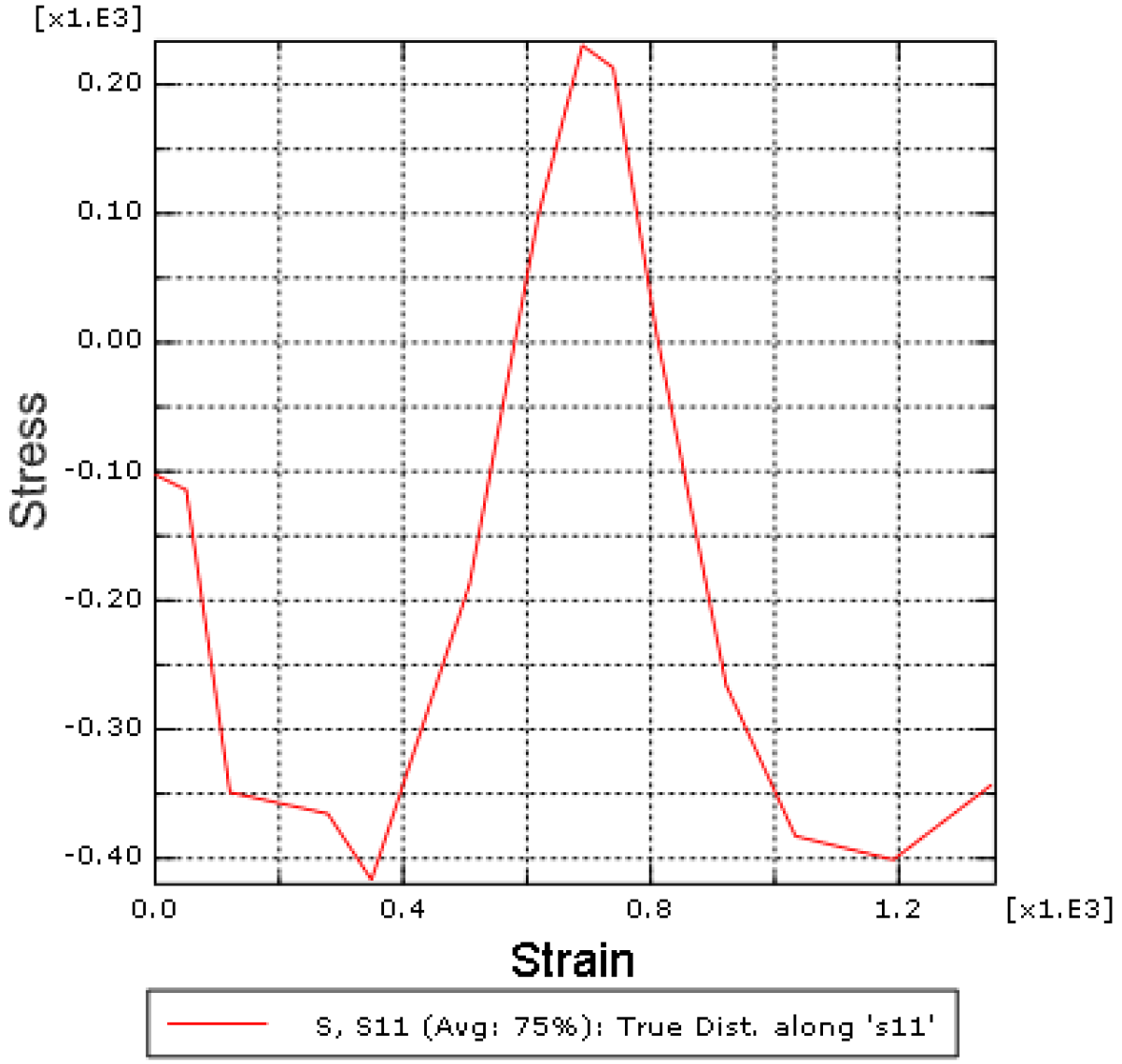

Figure 14: Von Mises shear-stress S11 deformations propagation

During the plastic stage of the shaft lining there is a combine action between the inner/outer steel cylinders and the concrete intermediate: both the structure elements are constrained and subject to a deformation. Before the structure failure, specific results for strain are obtains: ultimate load capacities equal to 40 MPa; the limit loop strain of steel and concrete varying between 4000 to 6000 $\mu\varepsilon$; the limit loop stress of steel is about 300 to 400 MPa, while for the concrete is about 150 to 200 MPa.

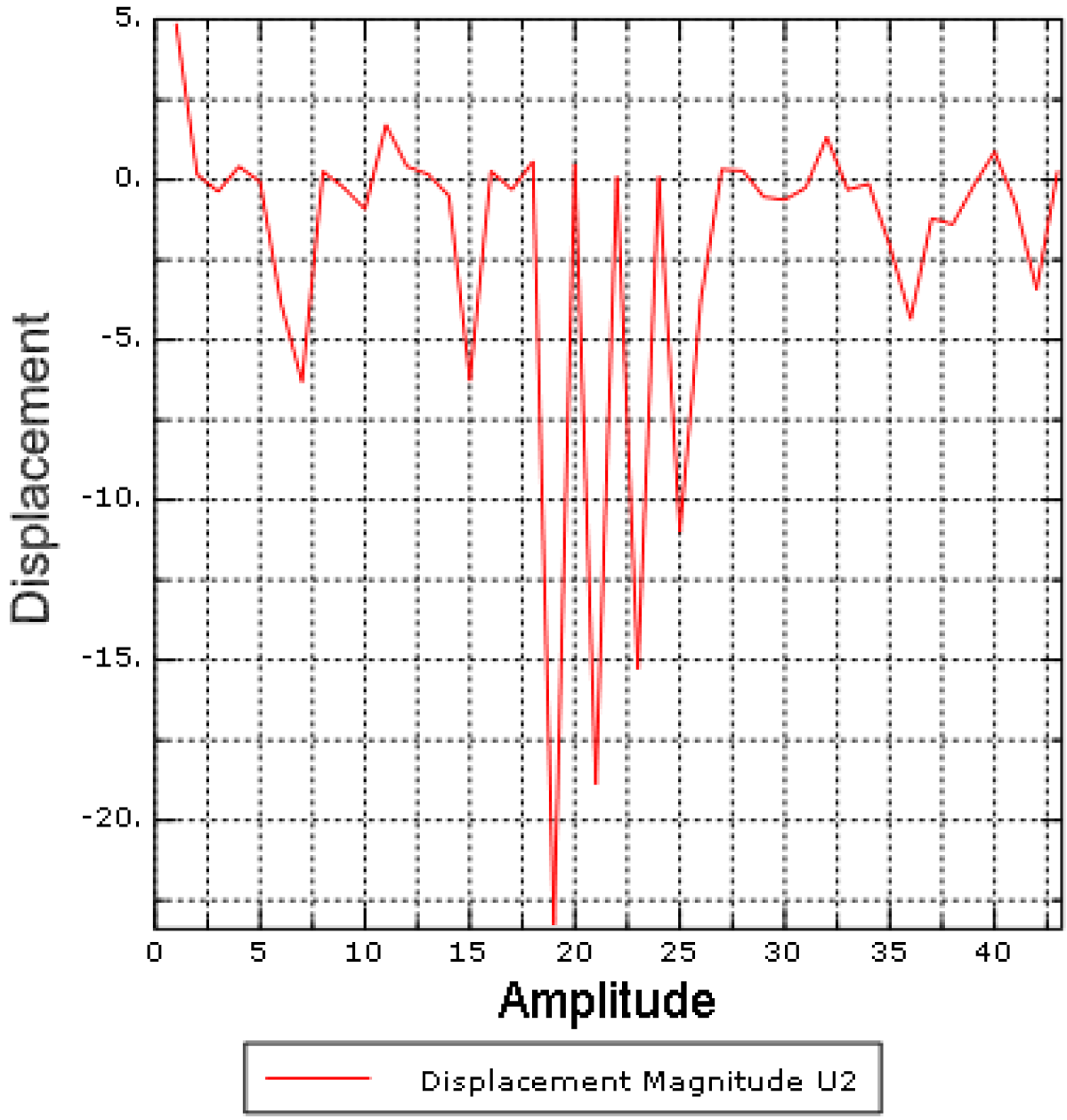

Figure 15: Displacement magnitude instability for the shaft linings

During the external load process the inner steel of the composite do not shows any radial confining forces due to the bi-axial compressive stress. The tensile deformation of the shaft lining structure can be explain here by the Poisson's effect; this is the weak structure point.

For the damaged structure the maximum hoop stress of the shaft lining reach the values of 300 MPa which exceed the numerical compressive strength of the concrete. During the loading process the concrete of the inner and outer of shaft lining model switch from the bidirectional to the three-dimensional compression state. The compressive strength of concrete will increase gradually under multiaxial stress conditions.

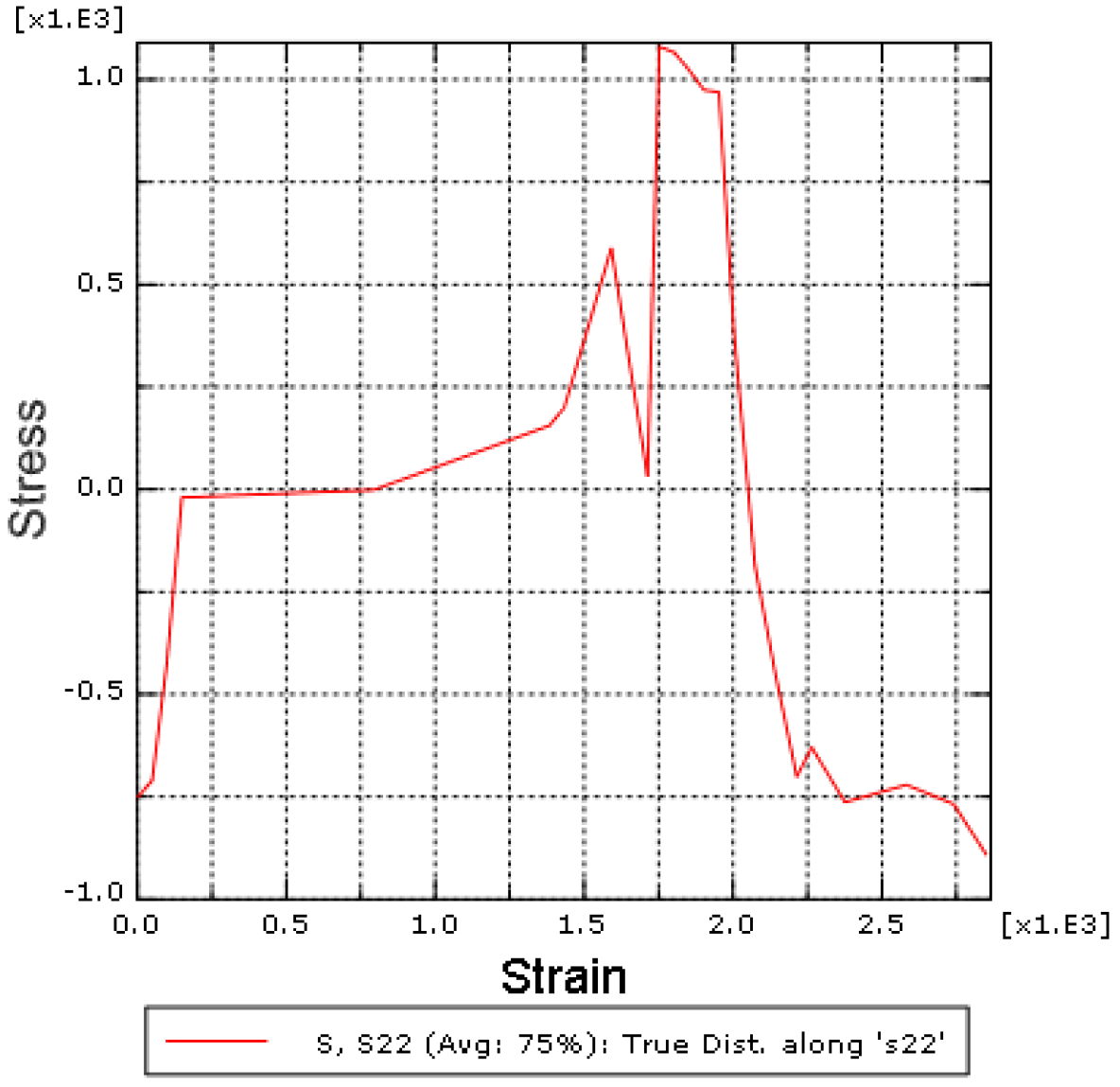

Figure 16: Von Mises shear-stress S22 deformations propagation

Notice that the shaft lining structure did not buckle at the plastic deformation stage; especially the inner steel cylinder of the composite. The inner and outer steel of the cylinder strongly contained the concrete (which is located at the intermediate composite layer) layer to avoid eventual crack and deformation. There is interesting plastic properties of the shaft lining structure during the concrete compressive strength increasing as show in Figures 6 and 7. The experimental data of the reference **[1]** verified the numerical data of the compressive strength for this research paper; the concrete hoop stress for all the nine specimens will increase higher and higher until the failure of the structure.

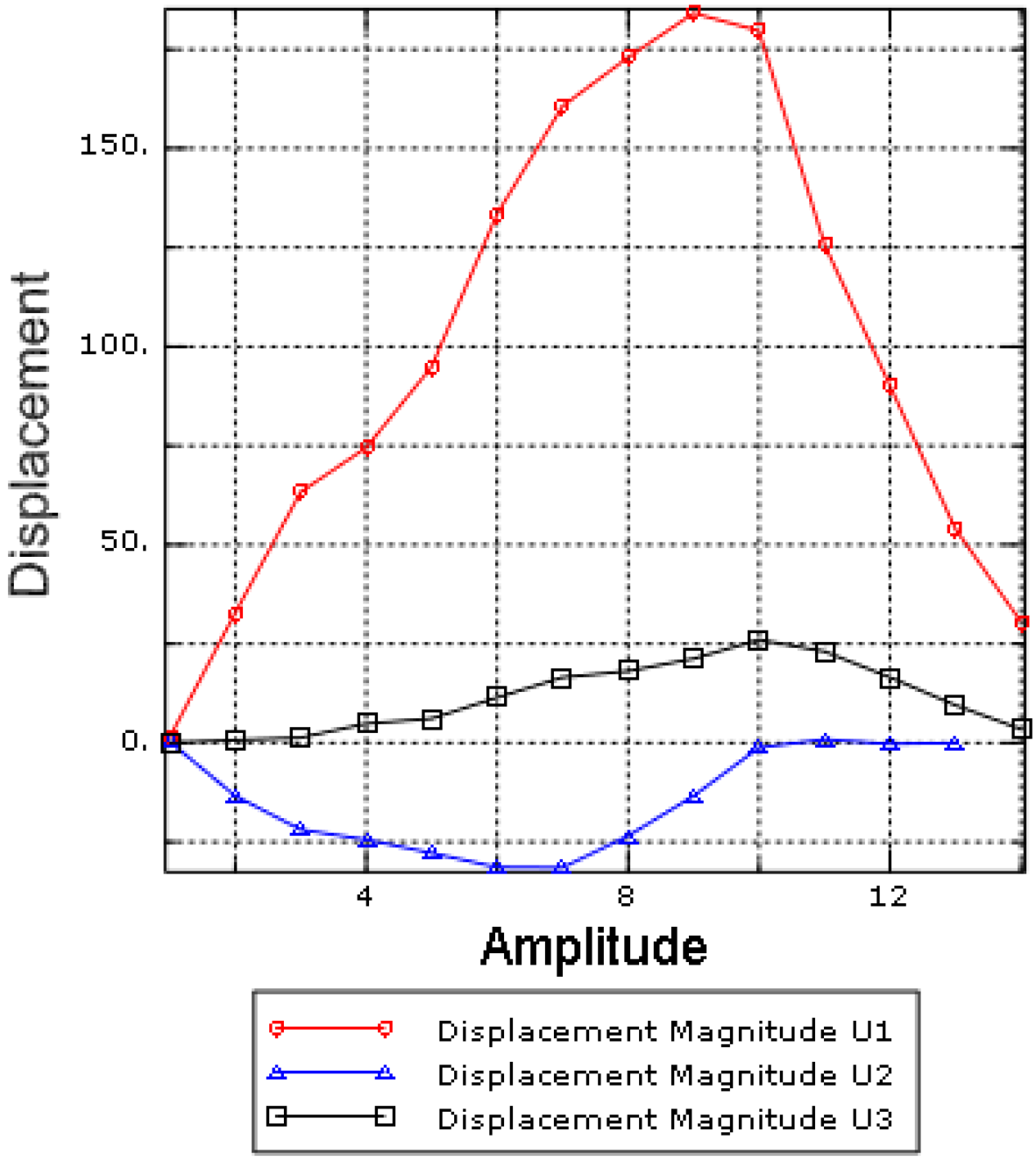

Figure 17: Magnitude instability for the deformations propagation of the structural element

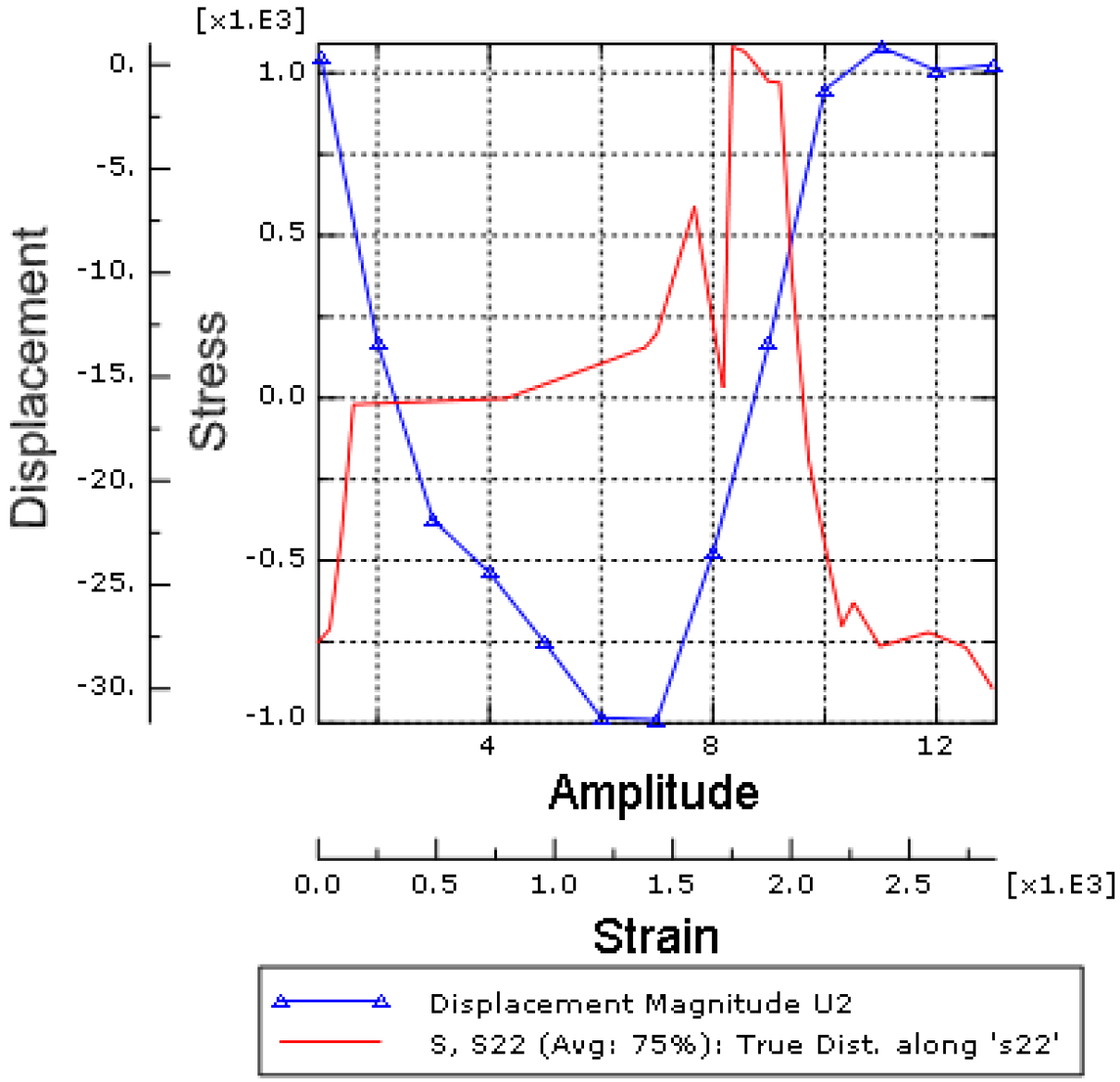

Figure 18: Engineering stress-strain behavior of the shaft lining composite structure steel-concrete for the specific concrete grade C70

The concrete grade C70 show optimums numerical results with a high bearing capacity compare to the two others concrete grade C65 and C75. We can conclude that the thickness diameter ratio has an impact on the structural properties of the shaft lining steel-concrete. For the specimens with a high thickness diameter ratio as for Z3, Z5 and Z7, we observe good results compared to others specimens: the

inner and outer thickness of the steel and concrete are the induct parameters of the shaft lining performances properties.

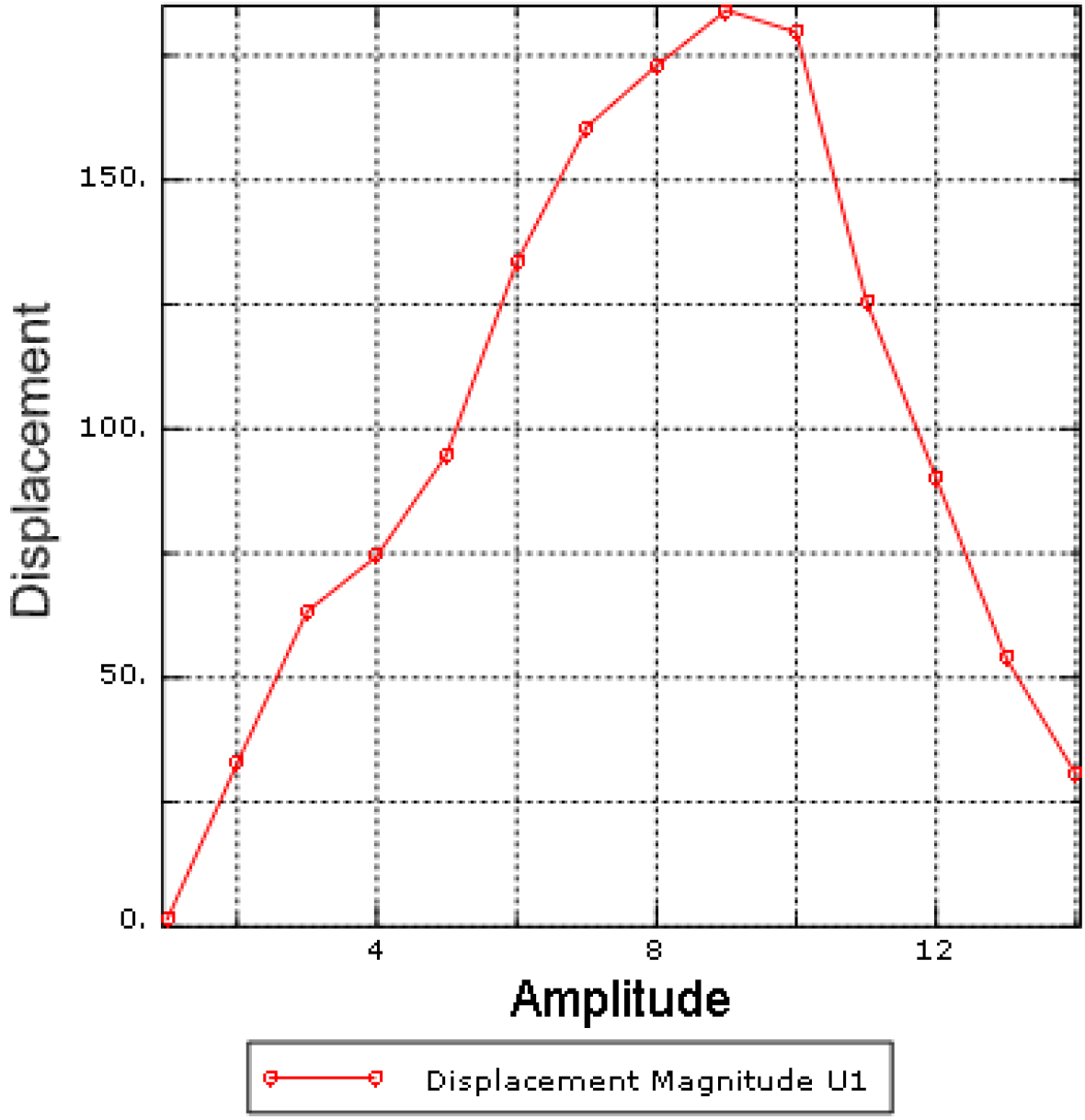

Figure 19: Normalized instability U1 deformation variation of the shaft lining structure

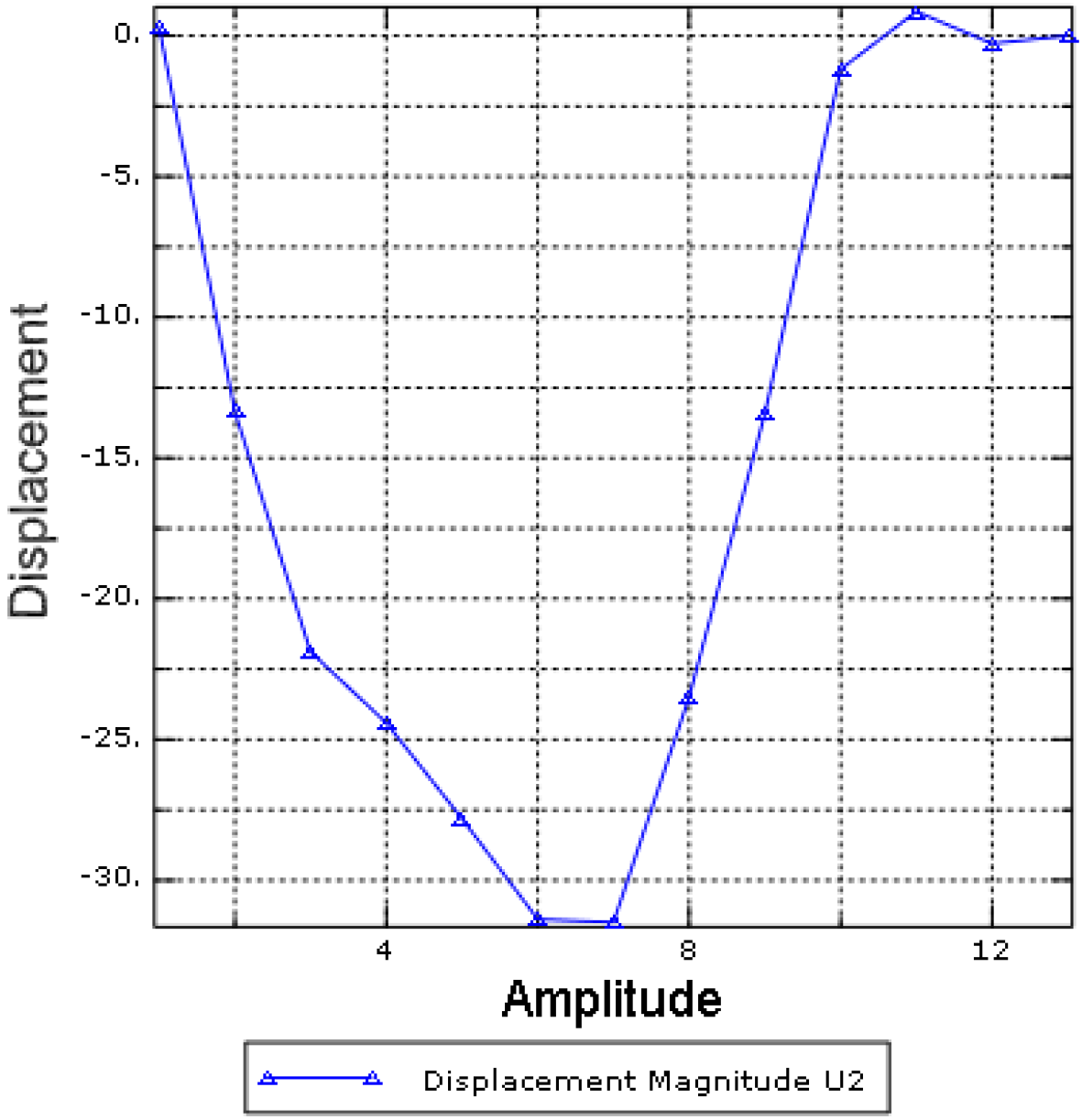

Figure 20: Normalized instability U2 deformation variation of the shaft lining structure

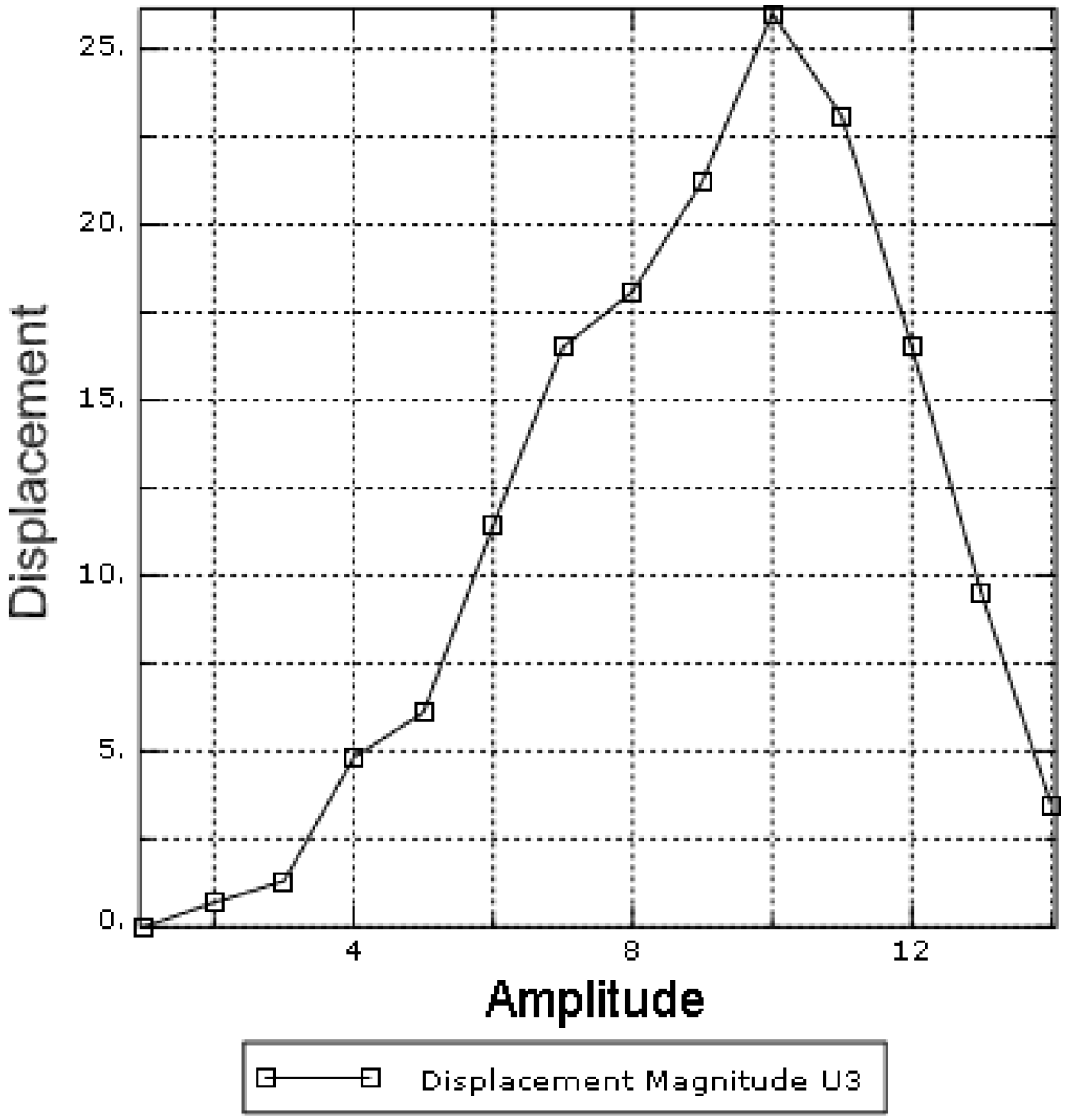

Figure 21: Normalized instability U3 deformation variation of the shaft lining structure

5. Conclusion

This research paper has endeavored to present the implementation of FEA using ABAQUS to predict the compressive damage effects and stress-strain response of nine shaft lining composites. Deformed configurations for the nine geometries obtained from the ABAQUS/Explicit dynamic simulation predicts the deformation mode accurately in all cases. Stress-strain response predicted by ABAQUS match well with experimental observations. The agreement between the numerical simulations and experimental findings demonstrates the overall accuracy and reliability of the analytical models in predicting the response of this new type of structural elements.

The concrete damaged plasticity model is used for the modelling of nonlinearity of the composite structure. The finite element modelling is the most challenging part of the research paper, especially the numerical modelling of concrete in shaft lining composite structures. The CDP model in this paper is also available in the ABAQUS finite element software but have been modified to improve the compressive stress-strain curve of the studied models. Also, the damaged variables are benefic for the new version of high-strength concrete C65, C70 and C75 under static loading. Numerical calculation is an effective method to study the bearing capacity of shaft lining structures. The nine studied shaft lining models reaches ultimate destructive state according to the development of the stress, strain and displacement of the FEM numerical results. It is crucial to noticed that the plastic displacement and the structure deformation notably influence the bearing capacity of shaft linings structures.

Based on the obtain results we can conclude that ABAQUS/Explicit predictions exhibit good correlation with experimental results. The FEM can find out the development process of strain and stress, but also allow us to understand and to follow the process of damage & failure surface of shaft lining composites

structures. So, the explicit dynamic analysis simulation can be included in a multi-stage analysis that includes the shaft lining manufacturing effects.

Availability of data and materials: All numerical setting data are presented in the article.

Competing interests: The author declare no competing interests.

Funding: None

Authors' contributions: The author read and approved the final manuscript.

Acknowledgements: We are grateful to PROF. ZHISHU YAO of the School of Civil Engineering and Architecture, Anhui University of Science and Technology, for have been provide the Experimental Data necessary for this Research Paper and also the Guidance and Methodology of this Research Paper; Thanks Also to Doctor XIANWEN HUANG of Singapore University for the Guidance and Methodology of the Research Paper.

Author details:

1. School of Civil Engineering and Architecture, Anhui University of Science and Technology, Huainan 232001, China

2. Department of Civil Engineering and Architecture, National Advanced School of Engineering, University of Maroua, Maroua, Cameroon

REFERENCES

[1] Yao, Z., Song, H., & Cheng, H. (2011). Test Study on Mechanical Characteristic of High Strength Composite Shaft Lining of Steel and Concrete. *Key Engineering Materials, 480-481*, 568 – 573 https://doi.org/10.4028/www.scientific.net/KEM.480-481.568

[2] J.C. Cuillière " Introduction à la méthode des éléments finis ", Éditions Dunod, Août 2011, ISBN 978-2100564385

[3] J.C. Cuillière " Introduction à la méthode des éléments finis -2ème édition ", Éditions Dunod, Janvier 2016, ISBN 978-2100742622

[4] A. Couture, V. François, J.C. Cuillière, P. Pilvin " Statistical Volume Element modeling based on the Unified Topology Model ", International Journal of Solids and Structures vol 191-192, pp 26-41, 2020 (doi: 10.1016/j.ijsolstr.2019.11.007)

[5] J.C. Cuillière, V. François, A. Nana, " Automatic Construction of Structural CAD Models from 3D Topology Optimization ", Computer Aided Design and Applications, vol 15 No 1, pp 107-121, 2018 (doi: 10.1080/16864360.2017.1353726)

[6] A. Nana, J.C. Cuillière, V. François, «Automatic reconstruction of beam structures from 3D topology optimization results ", Computers and Structures, vol 189 pp 62-82, 2017 (doi: 10.1016/j.compstruc.2017.04.018)

[7] P.H. Bischoff, S. Perry, Compressive behavior of concrete at high strain rates, Mater. Struct. 24 (6) (1991) 425–450

[8] M.S. Williams, Modeling of local impact effects on plain and reinforced concrete, Struct. J. 91 (2) (1994) 178–187

[9] H. Fu, M. Erki, M. Seckin, Review of effects of loading rate on concrete in compression, J. Struct. Eng. 117 (12) (1991) 3645–3659

[10] H. Fu, M. Erki, M. Seckin, Review of effects of loading rate on reinforced concrete, J. Struct. Eng. 117 (12) (1991) 3660–3679

[11] T. Jiang, et al., Three-dimensional nonlinear finite element modeling for bond performance of ribbed steel bars in concrete under lateral tensions, Int. J. Civ. Eng. (2020) 1–23

[12] V. Broujerdian, H. Karimpour, S. Alavikia, Predicting the shear behavior of reinforced concrete beams using nonlinear fracture mechanics, Int. J. Civ. Eng. 17 (5) (2019) 597–605

[13] A. Stolarski, Dynamic strength criterion for concrete, J. Eng. Mech. 130 (12) (2004) 1428–1435

[14] I. Carol, E. Rizzi, K. Willam, Formulation of anisotropic elastic degradation II. Generalized pseudo-Rankine model for tensile damage, Int. J. Solid Struct. 38 (4) (2001) 519–546

[15] L. Jason, et al., An elastic plastic damage formulation for concrete: application to elementary tests and comparison with an isotropic damage model, Comput. Methods Appl. Mech. Eng. 195 (52) (2006) 7077–7092

[16] J. Ju, Energy-based coupled elastoplastic damage theories: constitutive modeling and computational aspects, Int. J. Solid Struct. 25 (7) (1989) 803–833

[17] J. Lee, G.L. Fenves, Plastic-damage model for cyclic loading of concrete structures, J. Eng. Mech. 124 (8) (1998) 892–900

[18] J. Zhang, J. Li, Investigation into Lubliner yield criterion of concrete for 3D, simulation, Eng. Struct. 44 (2012) 122–127

[19] J. Lubliner, et al., A plastic-damage model for concrete, Int. J. Solid Struct. 25 (3) (1989) 299–326

[20] F. Lopez-Almansa, B. Alfarah, S. Oller, Numerical simulation of R.C. frame testing with damaged plasticity model. Comparison with simplified models, in: Second European Conference on Earthquake Engineering and Seismology, Istanbul, Turkey, 2014

[21] R.H. Evans, Effect of rate of loading on the mechanical properties of some materials, J. Inst. Civil Eng. 18 (7) (1942) 296–306

[22] T.V. Do, T.M. Pham, H. Hao, Dynamic responses and failure modes of bridge columns under vehicle collision, Eng. Struct. 156 (2018) 243–259

[23] G. Cusatis, Strain-rate effects on concrete behavior, Int. J. Impact Eng. 38 (4) (2011) 162–170

[24] M. Li, et al., Specimen shape and size effects on the concrete compressive strength under static and dynamic tests, Construct. Build. Mater. 161 (2018) 84–93

[25] Z. Ye, Y. Hao, H. Hao, Numerical study of the compressive behavior of concrete material at high strain rate with active confinement, Adv. Struct. Eng. 22 (10) (2019) 2359–2372

[26] J. Georgin, J. Reynouard, Modeling of structures subjected to impact: concrete behavior under high strain rate, Cement Concr. Compos. 25 (1) (2003) 131–143

[27] S. Park, Q. Xia, M. Zhou, Dynamic behavior of concrete at high strain rates and pressures: II. Numerical simulation, Int. J. Impact Eng. 25 (9) (2001) 887–910

[28] W. Zhou, et al., Mesoscopic simulation of the dynamic tensile behavior of concrete based on a rate-dependent cohesive model, Int. J. Impact Eng. 95 (2016) 165–175

[29] X. Chen, S. Wu, J. Zhou, Experimental and modeling study of dynamic mechanical properties of cement paste, mortar and concrete, Construct. Build. Mater. 47 (2013) 419–430

[30] L. Jin, W. Yu, X. Du, Effect of initial static load and dynamic load on concrete dynamic compressive failure, J. Mater. Civ. Eng. 32 (12) (2020), 04020351

[31] Y. Guo, et al., Response of high-strength concrete to dynamic compressive loading, Int. J. Impact Eng. 108 (2017) 114–135

[32] Y. Hao, H. Hao, Numerical evaluation of the influence of aggregates on concrete compressive strength at high strain rate, Int. J. Prot. Struct. 2 (2) (2011) 177–206

[33] Y. Hao, H. Hao, Influence of the concrete DIF model on the numerical predictions of R.C. wall responses to blast loadings, Eng. Struct. 73 (2014) 24–38

[34] M. Ferraioli, Dynamic increase factor for nonlinear static analysis of rc frame buildings against progressive collapse, Int. J. Civ. Eng. 17 (3) (2019) 281–303

[35] B. Alfarah, F. Lopez-Almansa S. Oller, New methodology for calculating damage variables evolution in Plastic Damage Model for R.C. structures, Eng. Struct. 132 (2017) 70–86

[36] Beton, CEB-FIP Model Code 1990: Design Code, Thomas Telford Publishing, 1993

[37] I. Concrete, Fib Model Code for Concrete Structures 2010, Ernst & Sohn publishing house2013, 2013

[38] R. Narayanan, A. Beeby, Designers' Guide to EN 1992-1-1 and EN 1992-1-2. Eurocode 2: Design of Concrete Structures: General Rules and Rules for Buildings and Structural Fire Design, vol. 17, Thomas Telford, 2005

[39] W. Dong, et al., Experimental study of equal biaxial-to-uniaxial compressive strength ratio of concrete at early ages, Construct. Build. Mater. 126 (2016) 263–273

[40] H. Cornelissen, D. Hordijk, H. Reinhardt, Experimental determination of crack softening characteristics of normal weight and lightweight, Heron 31 (2) (1986) 45–46

[41] W.W. Chen, B. Song, Split Hopkinson (Kolsky) Bar: Design, Testing and Applications, Springer Science & Business Media, 2010

[42] R. B. J. Brinkgreve, W. Broere. Plaxis V8 2D-Version 8 Material Model [M]. Dyer Volt Technology University, Plaxis, Netherlands

[43] YANG Hong Po. Numerical Studies on Bearing Capacity of Footings and Slope Stability by Reproducing Kernel Partial Method [D]. Zhejiang University 2008

[44] ZOU Guang-dian, JIANG Wan-ying. NUMERICAL SIMULATION OF ULTIMATE BEARING CAPACITY OF COMPLEX FOUNDATION [J]. ENGINEERING MECHANICS, 2005, 22 (2): 224-231

[45] S. Rizkalla, T. Hassan, and N. Hassan, "Design recommendations for the use of FRP for reinforcement and strengthening of concrete structures," Progress in Structural Engineering and Materials, vol. 5, no. 1, pp. 16–28, and 2003

[46] Ali Raza, Qaiseruz Zaman Khan, Afaq Ahmad, "Numerical Investigation of Load-Carrying Capacity of GFRP-Reinforced Rectangular Concrete Members Using CDP Model in ABAQUS", *Advances in Civil Engineering*, vol. 2019, Article ID 1745341, 21 pages, 2019

[47] L. C. Bank, Composites for Construction: Structural Design with FRP Materials, John Wiley & Sons, Hoboken, NJ, USA, 2006

[48] T. T. Nguyen, T. M. Chan, and J. T. Mottram, "Influence of boundary conditions and geometric imperfections on lateral-torsional buckling resistance of a pultruded FRP I-beam by FEA," Composite Structures, vol. 100, pp. 233–242, 2013

[49] G. Turvey and Y. Zhang, "A computational and experimental analysis of the buckling, post buckling and initial failure of pultruded GRP columns," Computers & Structures, vol. 84, no. 22-23, pp. 1527–1537, 2006

[50] A. Mirmiran, K. Zagers, and W. Yuan, "Nonlinear finite element modeling of concrete confined by fiber composites," Finite Elements in Analysis and Design, vol. 35, no. 1, pp. 79–96, 2000

[51] T. C. Rousakis, A. I. Karabinis, P. D. Kiousis, and R. Tepfers, "Analytical modelling of plastic behavior of uniformly FRP confined concrete members," Composites Part B: Engineering, vol. 39, no. 7-8, pp. 1104–1113, 2008

[52] A. I. Karabinis, T. C. Rousakis, and G. E. Manolitsi, "3D finite-element analysis of substandard RC columns strengthened by fiber-reinforced polymer sheets," *Journal of Composites for Construction*, vol. 12, no. 5, pp. 531–540, 2008

[53] B. Alfarah, F. López-Almansa, and S. Oller, "New methodology for calculating damage variables evolution in Plastic Damage Model for RC structures," *Engineering Structures*, vol. 132, pp. 70–86, 2017

[54] O. Youssf, M. A. El Gawady, J. E. Mills, and X. Ma, "Finite element modelling and dilation of FRP-confined concrete columns," *Engineering Structures*, vol. 79, pp. 70–85, 2014

[55] W. X. M. Liu and Z. Chen, "Parameters calibration and verification of concrete damage plasticity model of Abaqus," *Industrial Construction*, vol. 44, pp. 167–213, 2014

[56] Dassault Systems Simulia Corporation, *ABAQUS Analysis User's Manual 6.10-EF*, Dassault Systems Simulia Corporation, Providence, RI, USA, 2010

[57] V. K. Papanikolaou and A. J. Kappos, "Confinement-sensitive plasticity constitutive model for concrete in triaxial compression," *International Journal of Solids and Structures*, vol. 44, no. 21, pp. 7021–7048, 2007

[58] C. E. De Normalization, *Eurocode 2: Design of Concrete Structures—Part 1-1: General Rules and Rules for Buildings*, European Committee for Standardization, Brussels, Belgium, 2004

[59] J. B. Mander, M. J. N. Priestley, and R. Park, "Theoretical stress-strain model for confined concrete," *Journal of Structural Engineering*, vol. 114, no. 8, pp. 1804–1826, 1988

[60] P. Desayi and S. Krishnan, "Equation for the stress-strain curve of concrete," *ACI Journal Proceedings*, vol. 61, no. 3, 1964

[61] B. L. Wahalathantri, D. P. Thambiratnam, T. H. T. Chan, and S. Fawzia, "A material model for flexural crack simulation in reinforced concrete elements using ABAQUS," in *Proceedings of the First International Conference on Engineering, Designing and Developing the Built Environment for Sustainable Wellbeing*, Queensland University of Technology, Brisbane, Australia, April 2011

[62] A. S. Genikomsou and M. A. Polak, "Finite element analysis of punching shear of concrete slabs using damaged plasticity model in ABAQUS," *Engineering Structures*, vol. 98, pp. 38–48, 2015

[63] M. Elchalakani, A. Karrech, M. Dong, M. S. Mohamed Ali, and B. Yang, "Experiments and finite element analysis of GFRP reinforced geopolymer concrete rectangular columns subjected to concentric and eccentric axial loading," *Structures*, vol. 14, pp. 273–289, 2018

[64] J. Lee and G. L. Fenves, "A plastic-damage concrete model for earthquake analysis of dams," *Earthquake Engineering & Structural Dynamics*, vol. 27, no. 9, pp. 937–956, 1998

[65] G. Z. Voyiadjis and Z. N. Taqieddin, "Elastic plastic and damage model for concrete materials: Part I-theoretical formulation," *International Journal of Structural Changes in Solids–Mechanics and Applications*, vol. 1, no. 1, pp. 31–59, 2009

[66] N. F. Hany, E. G. Hantouche, and M. H. Harajli, "Finite element modeling of FRP-confined concrete using modified concrete damaged plasticity," *Engineering Structures*, vol. 125, pp. 1–14, 2016

[67] M. Z. Afifi, H. M. Mohamed, and B. Benmokrane, "Axial capacity of circular concrete columns reinforced with GFRP bars and spirals," *Journal of Composites for Construction*, vol. 18, no. 1, Article ID 04013017, 2013

[68] Q. Li, H. Meng, Dynamic strength enhancement of concrete-like materials in a split Hopkinson pressure bar test, Int. J. Solid Struct. 40 (2) (2003), 343–360

[69] J.I. Enem, J.C. Ezeh, M.S.W. Mbagiorgu, D.O. Onwuka Analysis of deep beam using Finite Element Method Int. J. Appl. Sci. Eng. Res., 1 (2012), pp. 348-356

[70] R. Malm. Predicting shear type crack initiation and growth in concrete with non-linear finite element method. PhD thesis, Department of Civil and Architectural engineering, Royal Institute of Technology (KTH) Stockholm, 2009

[71] Sofi, M., J.S.J. van Deventer, P.A. Mendis, and G.C. Lukey. "Engineering Properties of Inorganic Polymer Concretes (IPCs)." Cement and Concrete Research 37, no. 2 (February 2007): 251–257.

[72] ACI Committee 318, Building Code Requirements for Structural Concrete and Commentary, ACI 318-08, American Concrete Institute, Farmington Hills, 2008

[73] M. Andermatt, A. Lubell Behavior of concrete deep beams reinforced with internal fiber-reinforced polymer—experimental study ACI Struct. J., 110 (2013) pp. 585-594

[74] Juenger, Maria C.G., and Rafat Siddique. "Recent Advances in Understanding the Role of Supplementary Cementitious Materials in Concrete." Cement and Concrete Research 78 (December 2015): 71–80. doi:10.1016/j.cemconres.2015.03.018

[75] Razaqpur, A. Ghani, and Saverio Spadea. "Shear Strength of FRP Reinforced Concrete Members with Stirrups." Journal of Composites for Construction 19, no. 1 (February 2015): 04014025. Doi: 10.1061/(asce)cc.1943-5614.0000483

[76] Shahnewaz, Md, Robert Machial, M. Shahria Alam, and Ahmad Rteil. "Optimized Shear Design Equation for Slender Concrete Beams Reinforced with FRP Bars and Stirrups Using Genetic Algorithm and Reliability Analysis." Engineering Structures 107 (January 2016): 151–165. doi:10.1016/j.engstruct.2015.10.049

[77] Pantelides, Chris P., Michael E. Gibbons, and Lawrence D. Reaveley. "Axial Load Behavior of Concrete Columns Confined with GFRP Spirals." Journal of Composites for Construction 17, no. 3 (June 2013): 305–313. Doi: 10.1061/ (asce) cc.1943-5614.0000357